CENTRO BRASILEIRO DE PESQUISAS FÍSICAS

COORDENAÇÃO DE FÍSICA TEÓRICA

ON TOPOLOGICAL ANDERSON INSULATORS: FROM SDRG TO MACHINE LEARNING

Maria Daniela Leite de Souza

Rio de Janeiro, Brazil

May, 2019

Maria Daniela Leite de Souza

On topological Anderson insulators: from SDRG to Machine Learning

Dissertação apresentada ao Programa de Pós-Graduação em Física do Centro Brasileiro de Pesquisas Físicas, como requisito parcial para a obtenção do título de Mestra em Física.

Orientador: Tobias Micklitz
Coorientador: Linneu Holanda

May, 2019

CBPF 70 ANOS

MINISTÉRIO DA CIÊNCIA, TECNOLOGIA, INOVAÇÕES E COMUNICAÇÕES

"ON TOPOLOGICAL ANDERSEN INSULATORS: FROM **SDRG** TO MACHINE LEARNING"

MARIA DANIELA LEITE DE SOUZA

Dissertação de Mestrado em Física, apresentada no Centro Brasileiro de Pesquisas Físicas do Ministério da Ciência, Tecnologia, Inovações e Comunicações. Fazendo parte da banca examinadora os seguintes professores:

Tobias Micklitz - Presidente/Orientador

Wei Chen

Mucio Amado Continentino

Rio de Janeiro, 21 de maio de 2019.

Centro Brasileiro de Pesquisas Físicas
Rua Doutor Xavier Sigaud, 150, URCA, Rio de Janeiro, Brasil
Tel.: +55 21 2141-7100 CEP:22290-180
http://www.cbpf.br

Abstract

This thesis is about topological Anderson insulators. It is divided into two parts: one in which we study the so-called Strong Disorder Renormalization Group (SDRG) analysis of a disordered wire, and other in which we use a Neural Network that can recognize topological phases in clean insulators, with possibility of extension to disordered insulators. In the first part, we start with a review of the basic concepts about Anderson localization and one of the most known models for topological insulators (named the Su-Schriefer-Heeger - SSH - model). Then, we study a disordered wire with chiral symmetry, considering that the usual single parameter scaling hypothesis is violated, and introducing a second scaling parameter. Using the SDRG analysis, we show how to obtain the two-parameter flow diagram for this model. The second part, in its turn, addresses a brief picture to what is a Machine Learning algorithm and more precisely, one with a Feed-forward Neural Network (FNN) architecture. Our starting point is the question of how Machine Learning can be useful to classify topological phases of matter. We found the phase diagram of a clean insulator and extend the analysis for a disordered insulator.

Acknowledgements (in Portuguese)

Dedico este trabalho aos meus pais, João Bosco e Cícera Leite, pessoas à quem devo a vida e pelas quais tenho eterna gratidão. Obrigada por me terem dado a oportunidade de estudar, por me transferirem conhecimentos e valores que eu certamente levarei para toda a vida, e por acreditarem e confiarem em mim. Vocês são minha fonte de inspiração diária e meus melhores amigos. Este trabalho é também de vocês.

Aos meus irmãos, que apesar da distância, sei que torcem muito pelas minhas conquistas: Gabriela, por ser demasiado dócil, e Diêgo, que apesar de menos doçura, sei que tem um coração gigante. À minha pequena sobrinha Maria Júlia e minha cunhada, Juliana Teófilo. E também às pessoas da minha família que torcem pelo meu crescimento.

À minha irmã paraguaia, Bianca Galeano, que esteve ao longo dos últimos dois anos comigo compartilhando abraços, sorrisos, caminhadas, conselhos, e tantas outras coisas que tornaram a minha vida no Rio de Janeiro muito mais feliz. E ao Victor Martinez (*un grande boludo, pero el mejor boludo del mundo!*), pelas longas conversas e amizade que levarei para toda a vida. Vocês têm um espaço além de especial no meu coração!

À Josie Pereira, que mesmo sumindo (como típica carioca) sempre aparece nos momentos que eu mais preciso de boas conversas ou de algum conselho sincero. Obrigada por cuidar de mim, por torcer pelas minhas conquistas e por me dar bronca quando necessário. Enfim, obrigada por tudo!

À Letícia Moreira e Tássia Bezerra, duas mulheres incríveis que tanto me ajudaram nos meses iniciais de estadia no Rio. Compartilhar o 117 com vocês foi demasiado inspirador, fazendo-me crescer como pessoa e profissional. Ao Pablo

Ramón e Otacílio Vilar, muito obrigada por tornar o desafio de viver no 308 uma grande aventura. As comidinhas aos fins de semana e as angústias compartilhadas, foram decerto fundamentais ao longo dos últimos meses de desenvolvimento deste trabalho.

À Grecia Gomez, Riccardo Belvedere, aos casais Cavalcanti (Ivana e Erich) e Jáuregui (Gabriela e Máx), os meus agradecimentos pelos Domingos multiculturais, sorrisos, almoços e amizade. Pelas longas conversas e grandes aventuras, que me ensinaram e me ajudaram muito nos momentos de tensão.

Aos colegas de sala: Amanda Nicotina, Isadora Veeren, Guilherme Vieira, Filipe Melo (Filipinho) e Filipe Batista. Em particular, ao Gabriel Lando, pelas discussões filosóficas e por me introduzir ao mundo da escalada. A busca pelo esporte que mais me agrada foi consideravelmente otimizada após o seu impulso. Nesse sentido, agradeço ainda ao Fabio Cândido, pelas segs nas montanhas.

Aos amigos que o Cbpf me deu, sempre dispostos a discutir sobre Física, sobre a vida e sobre todo o resto: Phillipe, José (Zé), Gabrielzinho, Ana B., Jaime, Jade, Luci, Miguel, Pedrinho, Gisele, Fabrício, Guilherme, Bárbara Aguiar, e àqueles que não estão aqui listados, mas que contribuíram de forma direta ou indireta para o desenvolvimento deste trabalho.

Aos professores do CBPF, pela enorme disposição em ajudar os alunos a moldarem suas carreiras científicas. Em particular, ao Roberto Sarthour, Flávio Garcia, Ivan Santos, J. P. Sinnecker, José Helayël (que além de muita Física, me ensinou muto sobre a vida), Fernando Nobre, Fernando Melo, Mucio Continentino e Daniel Avalos.

E em especial, ao meu orientador Tobias Micklitz, a quem tenho enorme admiração e gratidão. Muito obrigada pela paciência quase infinita e disposição em me acompanhar ao longo de todo o Mestrado, me fazendo crescer muito como profissional. Obrigada ainda por ser uma pessoa tão humilde e por não ter desistido de mim ao longo desse processo.

Aos colegas Felipe Monteiro, Leo Cirto, Griffith Rufo, Sabrina Rufo, Nei Lopes e Linneu Holanda (co-orientador), pelas inúmeras discussões, pela paciência e disponibilidade em tirar dúvidas e compartilhar tantos conhecimentos. Vocês foram fundamentais para a produção deste trabalho.

September 3, 2019

No Ceará, na minha antiga universidade (a URCA), sei que há pessoas muito felizes com a produção deste trabalho. São elas: Eduardo Sousa, Julio Cesar, Claudio Dantas, Job Furtado, Romário Rafael e Laylson Vieira. Dedico este trabalho à todos vocês. Em particular, ao Prof. Augusto Nobre, por todas as boas conversas e mentoria; sua insistência me faz acreditar mais em mim mesma nos momentos de crise. Aos meus ex-orientadores Wilson Hugo, Apiano Morais e Carlos Emídio. E claro, às minhas irmãs de coração Khennya Maria e Rafaella Martins, que têm um espaço além de especial em meu coração (de pedra, como vocês mesmas dizem).

I also thank my collaborator and great friend Prof. Dr. Fidel Schaposnick. You are one of my main professional inspirations. Part of my conquers I owe you and to your deep dedication! Thanks for sharing great moments in Argentina, caring about me, and teach me much more than only Physics.

Another special thank to Felix Dangel, for becoming my confident in a very short time interval. Thanks for listening, talking and sharing experiences and virtual hugs, caring about our afternoon chats along the most chaotic months of my life.

Aos funcionários do CBPF, por tornarem todo o trabalho da instituição possível e nosso dia-a-dia muito mais eficiente: Bete e Ricardo, Cássio, Denise, Ana, Cheila e todos(as) funcionários(as) que se dedicam ao máximo para o bom funcionamento do Cbpf. E também às meninas do NIT-Rio, pelo belíssimo trabalho: Mariana Bottino, Patrícia, Neila e Monica.

À Capes pelo apoio financeiro.

September 3, 2019

Contents

Chapter 1

Introduction

Many physical systems contain different types of impurities and imperfections that naturally appear in the sample preparation process, influence the physical properties and are source of a rich phenomenology. These imperfections are generally referred to as disorder and understanding their impact is often challenging. In particular, for phase-coherent systems, quantum interference resulting from disordered scattering may lead to localization and consequently insulating behavior [1]. Indeed, in his seminal work of 1958, P.W. Anderson observed that the electron wave function in a three-dimensional system with a random potential completely changes upon increasing the disorder strength [2]. That is, the system undergoes a transition from a metallic phase at weak disorder - described by delocalized eigenstates and a finite probability to find the particle throughout the entire sample - to an insulating phase at strong disorder, where eigenfunctions are exponentially localized around some region in space.

The nature of this localization transition stayed unclear for almost 20 years until Thouless formulated in 1974 a scaling description of the localization problem of non-interacting electrons in static disorder potentials [3]. Two years later, Wegner conjectured the relation between this transition and the theory of critical phenomena for continuous phase transitions [4]. Finally, in 1979, Abrahams, Anderson, Licciardello, and Ramakrishnan, the so-called "gang of four", established a scaling theory of localization, which describes how the dimensionless conductance of a disordered single-particle system changes with increasing system size [5]. According to the sin-

gle parameter scaling theory for non-interacting electrons, all states are localized in a $d \leq 2$ phase coherent system in the thermodynamic limit. Localization induced by static disorder is by now a well established paradigm in condensed matter physics, and the resulting insulators are named Anderson insulators.

A different type of insulating behavior may be observed in clean single-particle systems and understood within the band theory of translational invariant systems. The band theory of electric conduction exists since the foundations of quantum mechanics. It explains, among many physical properties of solids, how crystalline materials are electric insulators, even with electrons hopping between the atoms [6]. For insulators, in particular, the eigenstates form energy bands separated by an energy gap where the lower band, the valence band, is completely filled and the creation of electron excitation thus requires energies overcoming the energy gap (see figure 1.1). For temperatures smaller than the gap such energy is not available and the electronic state is insulating.

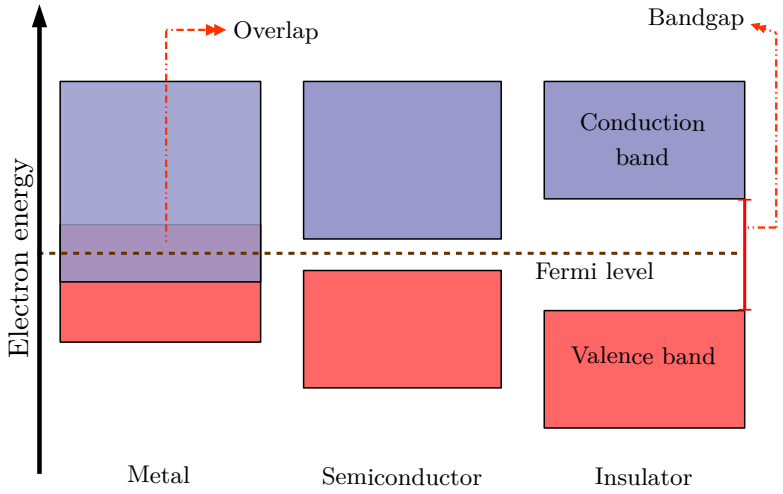

Figure 1.1: Scheme for conductance and valence bands in a metal, semiconductor and insulator (with the bandgap). Adapted from https://commons.wikimedia.org/wiki/File:Isolator-metal.svg.

It was realized only in 2005 that this is not the entire story and band insulators can come in different topological realizations. In their pioneering work, Kane and

Mele [7] realized that spin-orbit interactions in low energy electronic structures of graphene lead to a new variant of the Quantum Hall phase, named Quantum Spin Hall, which is characterized by a bulk energy band gap and gapless edge states on the boundary. In the same year, they showed that a nontrivial topological number can be associated to this phase [8], hence making it different from a normal insulator, e.g. resulting from intervally scattering. These works showed for the first time that topological trivial and non-trivial variants of band insulators can result from perturbing a semi-metal. The non-trivial variant is now called topological insulator. Soon after their first discovery, a periodic table for band insulators has been worked out, indicating in which systems (here characterized by the fundamental symmetries) and what space-dimension insulating behavior with non-trivial topology can occur [9].

At this point, a natural question arises, namely how topological band insulators get along with disorder. The first guess is that sufficiently strong disorder will destroy topological insulators: A crucial ingredient for the latter is the band gap which allows for the topological classification of band insulators. Disorder introduces mid-gap states that eventually create disorder bands, invalidating thus the necessary requirement of a bulk energy gap. On the other hand, in-gap states in low-dimensional systems are Anderson localized, and one may suspect that the notion of topology introduced for the band insulators may also survive in their Anderson insulating cousins. A famous example where this second scenario applies is the Quantum Hall effect. Historically, the discovery of the Quantum Hall (QH) effect in the 1980's introduced the idea that topology may play a central role in distinguishing electronic phases. It was observed that in the low temperature quantum limit the Hall resistivity assumes, differently from the classical behavior at high temperatures, only integers values. It is here worthy noting that a macroscopic and not microscopic physical property is quantized, hence stressing the importance of topology of quantum systems. By now it has been recognized that Quantum Hall insulators (close to the plateau transitions) are Anderson insulators with non-trivial topology, that is, the Anderson insulating variant of a topological insulator.

In this thesis we study topological Anderson insulators, which can occur in one-

dimensional systems with a specific lattice symmetry, labeled chiral symmetry. The thesis consists of two parts: In the first one we perform a Strong Disorder Renormalization Group (SDRG) analysis of a disordered wire with chiral symmetry. We derive the two-parameter scaling behavior which generalizes the single-parameter scaling of the "gang of four" to scenarios in which non-trivial topology plays a role. The SDRG is a powerful method to study the effect of disorder in quantum systems. It was first developed by D. S. Fisher [10]-[12] to study the ground state properties of disordered spin chains. In recent works, Mard, Hoyos, Miranda, and Dobrosavljevic [13] used the SDRG to analyse the scaling behaviour of a disordered wire with particle-hole/chiral symmetry, and observed that the usual single-parameter scaling was violated. However, they did not relate this unusual behaviour to the flow of a second relevant parameter: the (average) winding number accounting for non-trivial topological properties. Here, we show how one can incorporate this second flow parameter into the SDRG analysis and how this completes the picture, resulting in a flow diagram analogous to that of the Quantum Hall effect.

In the second part of the thesis, we take a different perspective and look at the problem of topological phases in disordered systems from a Machine Learning (ML) perspective. In the last years, the field of ML has appeared as a powerful alternative tool to study physical systems. Examples range from numerical solutions accelerating Monte Carlo simulations [14], classification of phases of matter [15], to the detection of entanglement [16] and many more. In particular, the problem of learning phases is quite challenging. In terms of a ML algorith, we can classify phases for categorizing information or use regression to predict continuous values, both cases are in general performed via supervised training. Topological phases of matter are in this context challenging since they are characterized by a manifestly non-local property, the topological number, while only local Hamiltonians are used as inputs. Specifically, we look for a ML algorithm which is able to classify non-trivial phases in disordered quantum wires with chiral symmetry. To make the problem richer we change from the single channel wires, considered in the first part of this thesis, to three-channel wires, since the latter allow for a larger number of different topologically non-trivial phases. We first derive the phase diagram of the

three channel wire as a function of hopping parameters and disorder strength from a self-consistent Born approximation for the disorder induced self-energy. We then train a Feedforward Neural Network on the clean wires using the eigenvectors of the Hamiltonian as input data, and study if the neural network can reproduce, in a next step, the phase diagram of the disordered system. This second part is not concluded yet, and we here only report our first results.

1.1 Outline

Since different approaches for topological Anderson insulators are studied within this work, it is divided into two parts. The first one addresses the SDRG analysis of a disordered wire along with chapters 2 and 3, while the second part contains a Machine Learning approach to the problem of classifying topological phases, on chapters 4 and 5.

Chapter 2 contains a brief introduction to the theory of Anderson localization, starting with a simple model of a one-dimensional quantum particle moving in a random potential, then using the transfer matrix formalism in order to compute transport properties in such system and performing some numerical experiments. The main ideas behind the single parameter scaling of localization and its limits of validity are also presented. To illustrate topological aspects, a review of the paradigmatic Su-Schrieffer-Heeger (SSH) model is discussed, including ideas about chiral symmetry and topological invariants.

The single channel disordered quantum wire is presented in chapter 3. In posses of the SDRG decimation rules, the topological invariant defined in terms of a generating function is calculated. Finally, the two-parameter scaling flow and a discussion of its properties is shown.

In chapter 4, the self-energies correction to the disordered topological invariant is presented. The target is to present a model for $N = 3$ connected chains, that has known phase diagram from the literature, for later comparison with the computed phase diagrams from our algorithm. This is the first step to the data generation process.

Chapter 5 addresses a brief introduction to Machine Learning algorithms, as well as a detailed description of data generation and numerical implementations. The last part contains conclusions and possible experiments to be explored in future works.

Part I

SDRG

Chapter 2

A brief introduction to localization and topological insulators

In this chapter, we review the two key concepts relevant for this thesis: Anderson localization and topological insulators.

First, we review the phenomenon of wave localization in random media within a simple tight-binding model for a disordered chain in section 2.1. To this end, we compare transmission coefficients of the chain, which is related to its conductance, in the classical and quantum limits. While in the classical limit strong dephasing suppresses any quantum interferences, the quantum limit is characterized by perfect phase coherence. This way we can see that the physical mechanism behind Anderson localization is the interference in multiple scattering paths. We support this analysis with some numerical experiments for this model.

In section 2.2 we discuss localization in higher dimensions by examining the effect of scaling on the conductance in a general d dimensional disordered system. We also discuss the main ideas underlying the scaling theory of localization, introduced by "the gang of four", following here a discussion in Ref. [5].

We then turn in section 2.3 to topological insulators. Concepts and properties of topological insulators, in their turn, are probably best accessed and understood within a concrete model. We, therefore, introduce the Su-Schrieffer-Heeger (SSH) model, which describes a one-dimensional system with staggered hopping amplitudes. It is one of the simplest models for a topological insulator, and we illustrate

how topological properties arise in one of its insulating phases.

2.1 Introduction to Anderson localization

Consider a one-dimensional non-relativistic particle of mass m initially prepared in a Gaussian wavepacket propagating along with some potential $V(x)$. The evolution of the wavefunction $\psi(x,t)$ is given by the Schrödinger's equation, that in one dimension reads

$$\left[-\frac{\hbar^2}{2m}\frac{\partial^2}{\partial x^2}+V(x)\right]\psi(x,t)=i\hbar\partial_t\psi(x,t). \tag{2.1.1}$$

We specify the potential V to a series of obstacles $j=1,2,...,N$ well separated and placed at randomly chosen distances

$$\Delta x_j=(x_j-x_{j-1}),$$

and each obstacle in its turn described by a potential $V_j(x)$ (see fig. 2.1).

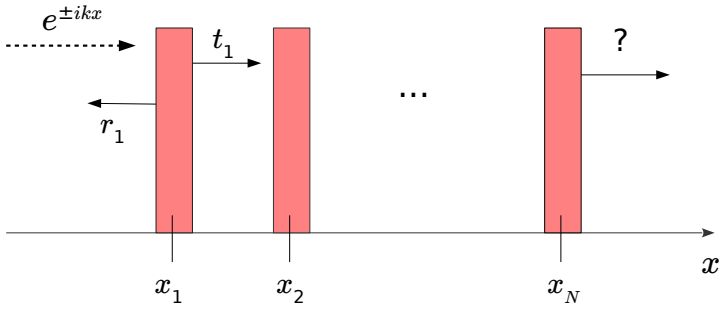

Figure 2.1: Each barrier $j=1,2,...,N$ is placed at x_i. The transmission and reflection coefficients are known for each scatter, and the question is to find the total transmission across all barries.

For simplicity let us first consider the case of a single scatterer at $x=0$. We then decompose the wavefunction with respect to the left (L, $x<0$) and right (R,

$x > 0$) side of the sample:

$$\psi(x) = \begin{cases} \psi_L(x) = \psi_L^{IN} e^{ikx} + \psi_L^{OUT} e^{-ikx} \\ \psi_R(x) = \psi_R^{OUT} e^{ikx} + \psi_R^{IN} e^{-ikx} \end{cases}, \tag{2.1.2}$$

where IN (OUT) means ingoing (outgoing) amplitudes at the sample (see fig. 2.2). These amplitudes are related by the reflection (r) and transmission (t) coefficients from the left side and r' and t' from the right side. So we have

$$\begin{aligned} \psi_R^{OUT} &= t\psi_L^{IN} + r'\psi_R^{IN} \\ \psi_L^{OUT} &= r\psi_L^{IN} + t'\psi_R^{IN} \end{aligned}. \tag{2.1.3}$$

In matrix form, the relations above can be written as

$$\begin{pmatrix} \psi_L^{OUT} \\ \psi_R^{OUT} \end{pmatrix} = \begin{pmatrix} r & t' \\ t & r' \end{pmatrix} \begin{pmatrix} \psi_L^{IN} \\ \psi_R^{IN} \end{pmatrix}, \quad \text{with} \quad S = \begin{pmatrix} r & t' \\ t & r' \end{pmatrix}, \tag{2.1.4}$$

where S is the scattering matrix relating incoming to outgoing amplitudes. Notice that the transmission and scattering coefficients are complex numbers, and the probabilities for reflection and transmission from the left are given by

$$R = |r|^2 = rr^*, \quad T = |t|^2 = tt^* \quad \text{and} \quad R + T = 1,$$

(equivalently from the right side).

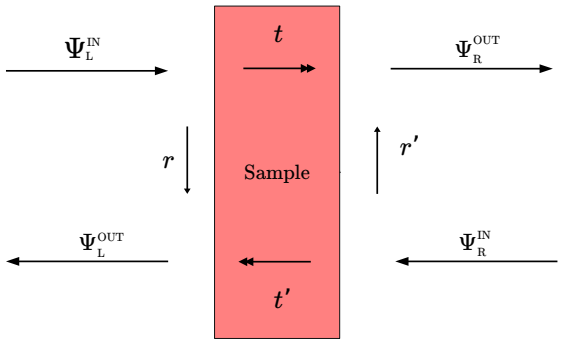

Figure 2.2: Scheme for ingoing/outgoing waves at the sample.

While the scattering matrix S allows for a very compact representation of the scattering at a single impurity, it becomes rather involved once we consider a series

of scatterers. In this case, it is more convenient to use a description in terms of the transfer matrix M, which follows a simple multiplication rule for scatterers in series. To see this, we decompose first the wavefunctions into right/left moving amplitudes, $\psi(x) = \psi^+ e^{ikx} + \psi^- e^{-ikx}$.

The transfer matrix M then maps the amplitudes from the left side of the scatterer to that of the right side of the scatter,

$$\begin{pmatrix} \psi_R^+ \\ \psi_R^- \end{pmatrix} = M \begin{pmatrix} \psi_L^+ \\ \psi_L^- \end{pmatrix}.$$

Rewriting 2.1.3, we have

$$\psi_L^{OUT} = \psi_L^- = r\psi_L^+ + t'\psi_R^- \quad \Longrightarrow \quad \psi_R^- = \frac{1}{t'}\psi_L^- - \frac{r}{t'}\psi_L^+ \tag{2.1.5}$$

and analogously for ψ_R^{OUT}. Combining both, we finally arrive at the the transfer matrix:

$$M = \begin{pmatrix} \frac{1}{t^*} & -\frac{r^*}{t^*} \\ -\frac{r}{t} & \frac{1}{t} \end{pmatrix}. \tag{2.1.6}$$

Since M maps the amplitudes from left to right across each scatterer, one can readily extend the scattering from a single impurity to several impurities in series. The total transfer matrix for N scatterers is simply obtained from multiplying transfer matrices M_i for the i-th scatterer,

$$M_{12...N} = M_N M_{N-1} ... M_2 M_1.$$

In an experiment with two barriers (fig. 2.3) $M_{12} = M_2 M_1$, and we find

$$t_{12} = \frac{t_1 t_2}{1 - r_1' r_2}. \tag{2.1.7}$$

The physical meaning of eq. (2.1.7) becomes more clear if we expand the right-hand side in a power series

$$t_{12} = t_1 \left[1 + r_2 r_1' + (r_2 r_1')^2 + (r_2 r_1')^3 + ...\right] t_2. \tag{2.1.8}$$

That is, the transmission amplitude is given by the sum of the contributions of all possible paths γ trough the two barriers,

$$t_{12} = \sum_{\gamma: 1 \to 2} t_\gamma \tag{2.1.9}$$

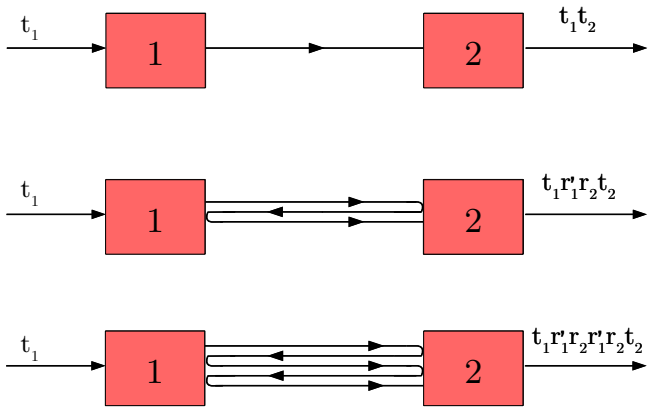

Figure 2.3: Scheme of the transmission across two barriers. Notice that the amplitude t_{12} contains terms from all possible paths.

where the paths can be organized in the number of the internal reflections. So, in the simplest path γ_0, the particle just propagates through the two potentials $t_{\gamma_0} = t_1 t_2$, in the first nontrivial path there is one internal reflection $t_{\gamma_1} = t_1 r_2 r_1' t_2$, etc. We then recall that the transmission probability is given by the square of the amplitude, and can be organized as follows

$$T_{12} = \sum_{\gamma,\gamma'} t_\gamma t^*_{\gamma'} = \sum_{\gamma} t_\gamma t^*_{\gamma} + \sum_{\gamma \neq \gamma'} t_\gamma t^*_{\gamma'}. \tag{2.1.10}$$

In the expression above, the first contribution describes the classical transmission probability, while the second contribution sums all the quantum interference corrections to it. We next discuss that the latter drastically changes the transmission probability through a series of N randomly placed scatterers.

2.1.1 Clasical limit

Let us first consider the classical limit in which strong dephasing is present and the quantum interference corrections are strongly suppressed. One then finds the transmission probability to propagate through two impurities

$$T_{12} \simeq \sum_{\gamma} t_\gamma t^*_{\gamma} \tag{2.1.11}$$

The geometric series then gives

$$T_{12} = \frac{T_1 T_2}{1 - R_1 R_2}, \tag{2.1.12}$$

where T_i and R_i are, respectively, the total transmission and reflection probabilities for each scatter i.

The element resistance of the obstacles, defined as $(1-T)/T$, is calculated with the classical transmission and sums in series classical behavior,

$$\frac{1-T_{12}}{T_{12}} = \frac{1-T_1}{T_1} + \frac{1-T_2}{T_2}. \tag{2.1.13}$$

Across N identical impurities distributed with density $n = N/L$, the classical resistance grows like

$$\frac{R}{T} = N\frac{R_1}{T_1} =: \frac{L}{l_1}, \tag{2.1.14}$$

in which $l_1 = T_1/(nR_1)$ characterizes the backscattering strength of a single impurity. Equation 2.1.14 simply states that the total classical resistance of a wire grows linearly with its length L. This result is known as Ohm's law and reflects that the classical dynamics of the particle is diffusive.

2.1.2 Anderson localization

Consider now the opposite limit of perfect phase coherence, where the quantum interference correction have to be accounted for. Again, in case of two scatterers, the transmission probability now reads

$$T_{12} = \frac{T_1 T_2}{|1-\sqrt{R_1 R_2}e^{i\theta}|^2}. \tag{2.1.15}$$

The difference with respect to the classical limit (in 2.1.12) is in the denominator, where the phase $e^{i\theta}$ marks a difference between the classical and quantum mechanical limits and has a straightforward interpretation: It simply accounts for accumulated dynamical phase during the internal reflection of the particle. While this latter looks rather innocent it becomes very involved once N randomly placed scatterers are considered.

In this case, the interference corrections will come with multiple phase factors accumulated during propagation in between the randomly placed scatterers. This random distances makes the phase factors randomly distributed in the interval $[0, 2\pi]$ independently of the reflection phases, and a calculation of T looks very complicated.

However, the randomness can be taken as an advantage, once we consider the logarithm of the transmission. Across long samples, when one averages the logarithm in (2.1.15), the denominator drops out, since

$$\int_0^{2\pi} \frac{d\theta}{2\pi} \ln|1 - \sqrt{R_1 R_2} e^{i\theta}| = 0, \tag{2.1.16}$$

and so $\langle \ln T \rangle$ is additive: the total extinction of a channel with length L grows like $|\langle \ln T \rangle| = nL|\ln T_1|$. With this scaling behavior, the log-averaged transmission drops fast by increasing the length L,

$$\exp(\langle \ln T \rangle) = e^{\frac{-L}{\xi_{loc}}}. \tag{2.1.17}$$

Recalling that the transmission is related to the conductivity, we conclude that the conductance in the fully phase-coherent regime becomes exponentially small. Quantum interference thus drastically changes the classical diffusion: The particle becomes Anderson localized.

The characteristic length scale for Anderson localization is the localization length

$$\xi_{loc} = \frac{1}{n|\ln T_1|}. \tag{2.1.18}$$

For weak scattering, $nl_1 = T_1 R_1^1 \gg 1$, and $|\ln T_1| \approx (nl_1)^{-1}$, with localization length $\xi_{loc} = l_1 = 2l$. In one dimension, no matter how weak is the disorder, all states will localize due to quantum interference. We will see in section 2.2 how this conclusion can be also derived from a single parameter scaling hypothesis.

2.1.3 Numerical experiments in 1d

In this section, we perform two numerical experiments of the $1d$ Anderson model. All codes are written in Python3 and the detailed scripts for this chapter can be found at https://github.com/Danielaleite. Here, we use the following parameters: the energy (E), the system size (L) and the number of realizations N.

Up to this point, we used the transfer matrix formalism to combine the discrete scatters with the proper phases in a model of a propagating wave along a continuous $1d$ axis. We can also go further and build a discrete model in a $1d$ lattice, whose

Hamiltonian is given by

$$H = \sum_{-\infty}^{+\infty} \left(\varepsilon_n |n\rangle\langle n| + t|n\rangle\langle n+1| + t|n+1\rangle\langle n|\right), \tag{2.1.19}$$

where $|n\rangle$ describes the occupation of site n and on-site energies ε_n are randomly drawn from some gaussian distribution, and the hopping t is set to have energy units ($t = 1$). If ε_n is zero, the system is translational invariant and eigenstates are discrete plane waves $\psi_n = e^{ikn}$, where k is the wavenumber and $k \in [-\pi, \pi[$. The dispersion relation is $E(k) = 2\cos k$. We introduced disorder considering ε_n as a random variable, distributed along the interval $\varepsilon_n \in [-W/2, W/2]$ [1].

In the first numerical experiment, we diagonalized the Hamiltonian 2.1.19 on a finite lattice. Plot in fig. 2.4 contains an example of a typical localized wavefunction of a given state with energy $E = 0.005$.

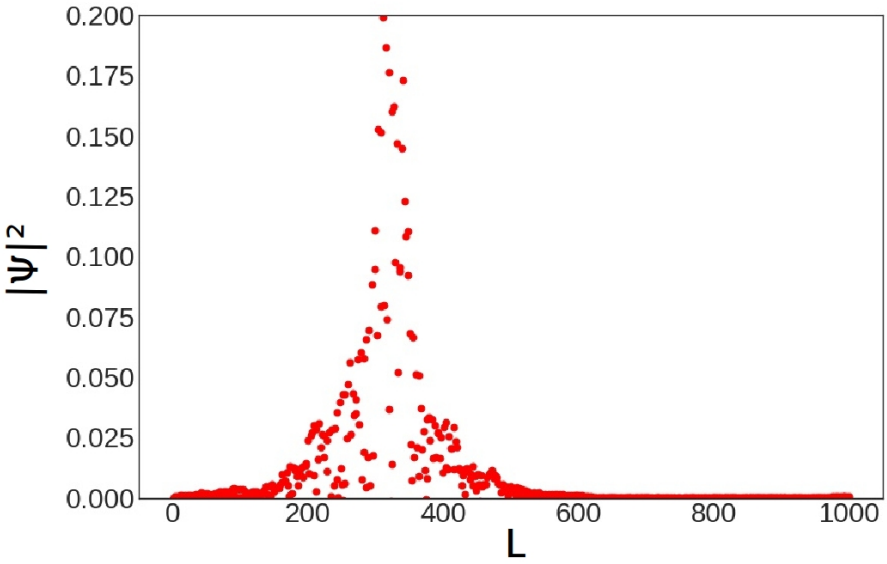

Figure 2.4: We notice that the eigenstates are localized in the presence of disorder. In this example, we used $W = 1$, $L = 1000$ and energy $E = 0.005$.

We also estimated the localization length using the Inverse Particpation Ratio (IPR), which is defined for each eigenstate by

$$\text{IPR} = \sum_i |\psi_i|^4.$$

Essentially, this value carries all information about the localization properties of the quantum state. The figure 2.5 shows how this ratio changes in terms of the energy, and a comparision with the estimated localization length.

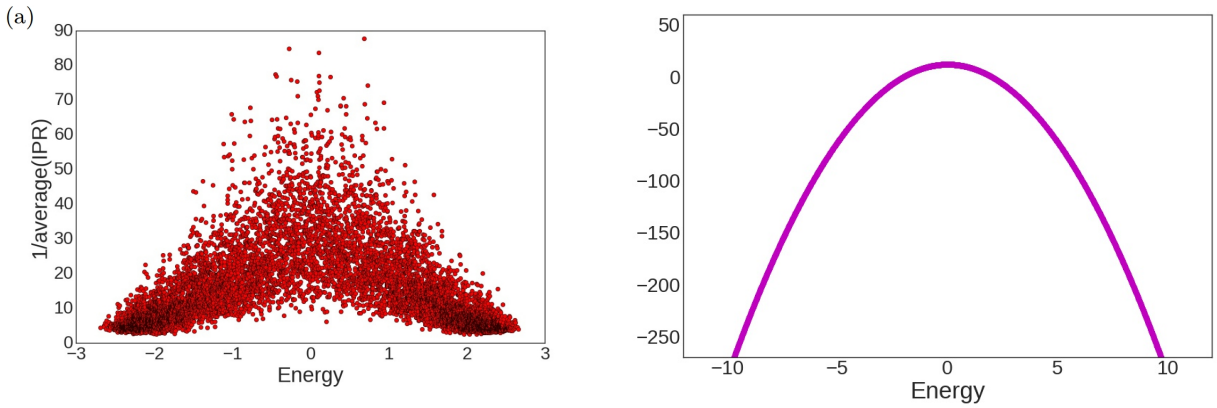

Figure 2.5: Numerical experiments of the $1d$ Anderson model: IPR vs. energy in the (a) experimentand (b) Theory.

In a second experiment, we computed the intensity $\ln|\psi_n^2|$ for a given realization of disorder. Starting from the reduced form of time-independent Schröedinger equation for an eigenstate $|\psi\rangle = \sum_n \psi_n|n\rangle$, with energy E, we have

$$\varepsilon_n|n\rangle\langle n|\psi_n|n\rangle + |n\rangle\langle n+1|\psi_n|n\rangle + |n+1\rangle\langle n|\psi_n|n\rangle = E\psi|n\rangle \tag{2.1.20}$$

$$\varepsilon_n\psi_n|n\rangle + \psi_{n-1}|n\rangle + \psi_{n+1}|n\rangle = E\psi|n\rangle, \tag{2.1.21}$$

that lead us to a recursive relation

$$\psi_{n+1} = (\varepsilon_n - E)\psi_n - \psi_{n-1}. \tag{2.1.22}$$

We solved eq. 2.1.22 at some arbitrary energies and with periodic boundary conditions ($\psi_n = 1$ and $\psi_{n+1} = e^{ik}$), describing an outgoing wavevector k and amplitude 1. We plot the intensity $\ln|\psi_n|^2$ in figure 2.6.

2.2 Scaling theory of localization

In this section, we present some of the key ideas behind the single parameter scaling hypothesis, guided by the approach in Ref. [5].

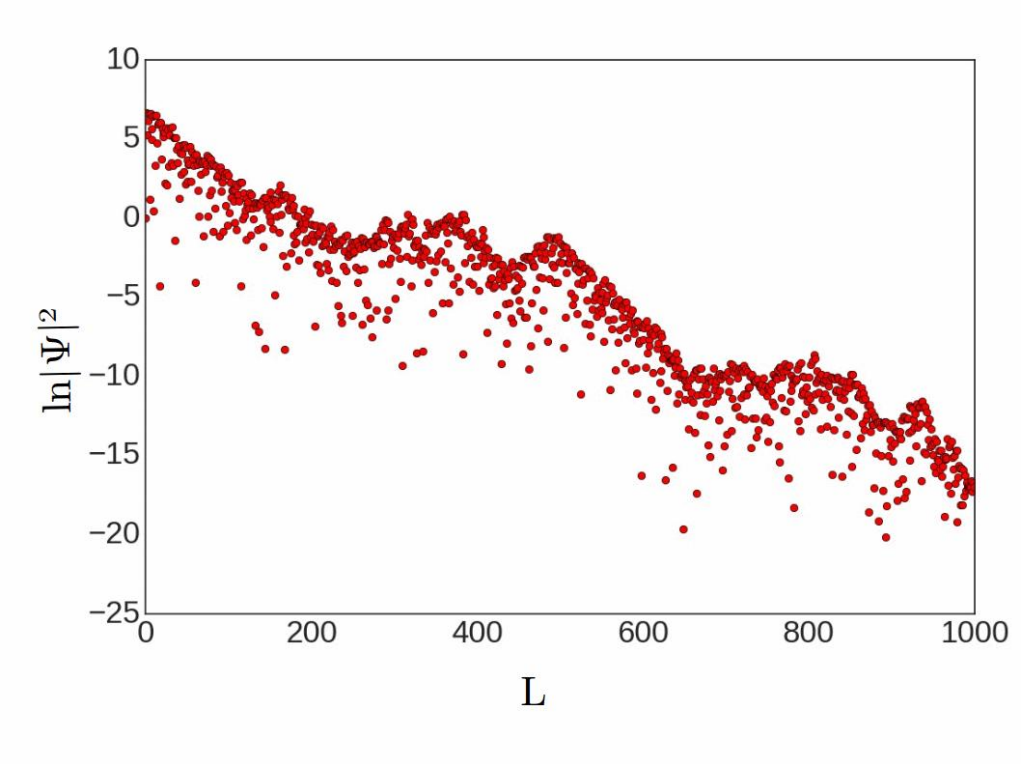

Figure 2.6: The intensity $|\psi_n|^2$ decays exponentially for one realization of disorder. Here, we set $L = 1000$, $W = 1$ and $E = 0.5$.

A scaling theory describes how relevant physical properties of a system change under a change of its size. It is one of the most influential applications of renormalization group ideas. In 1979, the "gang of four" composed by Abrahams, Anderson, Licciardello and Ramakrishnan [5] proposed a scaling theory of localization in the context of transport properties of disordered conductors. Traditionally, this theory is formulated in terms of a dimensionless parameter, namely the dimensionless conductance or "Thouless number" [5], defined as

$$g(L) = \frac{G(L)}{(e^2/2\hbar)}, \tag{2.2.23}$$

where $\hbar$ is the Planck's constant, e the elementary charge, L is the size of the system (in the original approach of the gang of four, the system is a finite hypercube) and $G(L)$ is the system conductance, defined by

$$G(L) = \sigma L^{d-2}, \tag{2.2.24}$$

and σ is the conductivity of the system. They suggested that scaling properties

of the conductance are determined by a single parameter - the conductance itself - through a scaling equation

$$\frac{d(\ln g)}{d(\ln L)} = \beta(g). \tag{2.2.25}$$

Notice that if β is positive ($\beta > 0$), L grows as we increase g and the system goes to a conducting phase. If β is negative ($\beta < 0$), g decreases by increasing L and the system flows to an insulating phase. When $\beta = 0$, the system is at a phase transition point.

We can get asymptotic behaviour of β for both large and small g, from general physical arguments [5]. For large g, from eq. 2.2.24, we have

$$\lim_{g\to\infty} \beta(g) = d - 2. \tag{2.2.26}$$

In the other limit $g \to 0$, the exponencial localization is valid, then g falls off exponentially: $g \sim e^{-\alpha L}$, with α being the inverse of the localization length. So we have

$$\lim_{g\to 0} \beta(g) \sim \ln g < 0. \tag{2.2.27}$$

From these asymptotics limits, we can build a curve for β in dimensions $d = 1, 2$ and 3. To do so, we need to assume that this curve is: (i) monotonic and (ii) continuous. Regarding the dimensions, according to eq. 2.2.26, if $d = 1$, no matter how large is g, the β function is always negative, so the β-flow is to an insulating phase. If $d = 2$, $\beta = 0$ and the prediction is that all states are localized, so the flow is also to an insulating phase. In $d = 3$ dimensions, we have $\beta(g) > 0$ for large values of g and $\beta(g) < 0$ for small values of g. So, there is a critical point - where $\beta = 0$ - that separates these behaviours, and the flow goes to either metallic or insulating phase. Figure 2.7 summarizes these behaviours.

We will see in the next chapter that the scaling ideias are challenged in the context of topological systems. The assumption that scaling properties of conductance are governed by only one parameter is not valid in such systems anymore, and it is necessary to introduce a second scaling parameter. In fact, the appearence of a second scaling parameter was suggested first for the integer Quantum Hall effect, where an insulating state has a non-trivial topology. Specifically, Pruisken and Khmelnitskii proposed in 1988 that the diagonal and off-diagonal elements of the

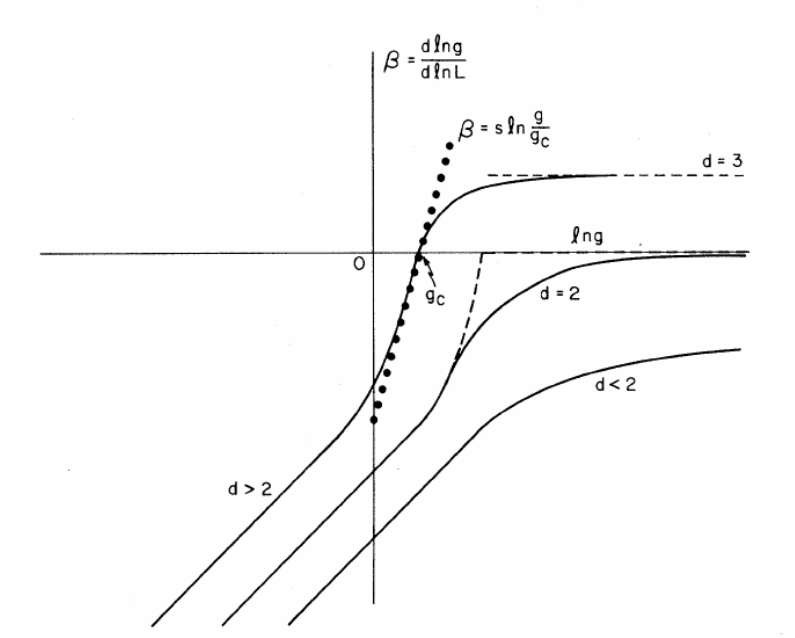

Figure 2.7: Qualitative behaviour of $\beta(g)$ in dimensions $d = 1, 2, 3$. Taken from [5].

dimensionless conductance tensor $g = g_{xx}$ and $g_H = g_{xy}$ [24] are the relevant parameters determining the β function in this case. At this point, it is convenient to introduce the main ideas behind topological systems.

2.3 Su-Schrieffer-Heeger (SSH) model

The Su-Schrieffer-Heeger (SSH) model [21] is one of the simplest to understand the physical properties of a one-dimensional topological system. It is a tight-binding model that exhibits a topological phase transition, and was first proposed to describe topological solitons in polyacetylene, a linear polymer composed by quasi-1d chains of Carbon-Hydrogen monomers (see figure). The spinless fermions can hop in the chain (1d lattice) with alternating amplitudes. In this section, we describe this model and introduce some relevant concepts as the chiral symmetry and topological number. The material presented throughout this section is guided by the approach in Ref. [6].

We consider a 1d chain with $2N$ sites and spinless fermions described by the

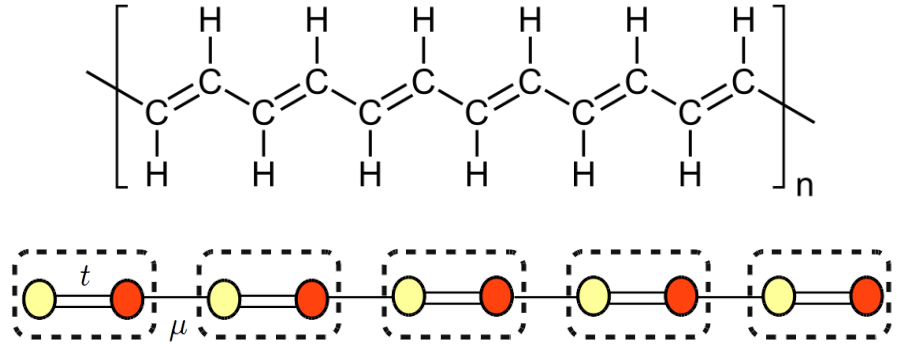

Figure 2.8: Origin and geometry of the SSH model. Configuration of polyacetilene molecule (above), and scheme for a 1D chain with two atoms in a unit cell, with alternating hopping amplitudes t (double line) and μ (single line) intra-cell and inter-cell, respectively.

following Hamiltonian

$$\hat{H} = \sum_{i=1}^{2N} t_i \hat{c}_i^\dagger \hat{c}_{i+1} + \text{h.c.} \tag{2.3.28}$$

where "h.c." means hermitian conjugate, $c_i^\dagger$ is the operator that creates a fermion on site $i = 0, 1, ..., 2N$, and t_i is the hopping amplitude. This model has no onsite potential terms and we assume periodic boundary conditions ($\hat{c}_{2N+1}^\dagger \equiv c_1$). The hopping amplitudes alternate between "weak" and "strong" hopping, so it's more convenient to change the notation to $t_{2i} = t$ and $t_{2i+1} = \mu$, indicating even and odd links,

$$\hat{H} = \sum_{i=1}^{2N} \left(t \hat{c}_{2i-1}^\dagger \hat{c}_{2i} + \mu \hat{c}_{2i}^\dagger \hat{c}_{2i+1} + \text{h.c.} \right) \tag{2.3.29}$$

We can think of the system as an N site lattice with a two-component unit cell (i.e. containing the two sites), which implies that it is described by two energy-bands. If the latter are separated by a gap throughout the entire Brillouin zone, the system is in an insulating phase.

Building on the two-component unit cell picture, it is convenient to introduce

$$\hat{\mathbf{c}}_i^\dagger = (\hat{c}_{i,1}^\dagger, \hat{c}_{i,2}^\dagger) = (\hat{c}_{2i-1}^\dagger, \hat{c}_{2i}^\dagger), \tag{2.3.30}$$

where i labels the cell index. Rewriting the Hamiltonian in this new notation

$$\hat{H} = \sum_{i=1}^{N} \left(t \hat{c}_{i,1}^\dagger \hat{c}_{i,2}^\dagger + \mu \hat{c}_{i,2}^\dagger \hat{c}_{i+1,1}^\dagger + \text{h.c.} \right) = \sum_{i=1}^{N} \hat{c}_i^\dagger H_{ij} \hat{c}_j. \tag{2.3.31}$$

Each component H_{ij} is now a (2×2) matrix, and we will name $T_i = H_{i,i+1}$ hopping matrices, and $U_i = H_{ii}$ onsite potentials. In a chain with 4 cells (8 sites), for example, the entire Hamiltonian matrix H takes the form

$$H = \begin{bmatrix} U_1 & T_1 & 0 & T_4^\dagger \\ T_1^\dagger & U_2 & T_2 & 0 \\ 0 & T_2^\dagger & U_3 & T_3 \\ T_4 & 0 & T_3^\dagger & U_4 \end{bmatrix}, \quad \text{where} \quad U = \begin{bmatrix} 0 & t \\ t^* & 0 \end{bmatrix} \quad \text{and} \quad T = \begin{bmatrix} 0 & 0 \\ \mu & 0 \end{bmatrix}. \tag{2.3.32}$$

We can write onsite and hopping matrices in terms of the Pauli matrices

$$U = t\sigma_x, \qquad T = \frac{\mu}{2}(\sigma_x - i\sigma_y), \tag{2.3.33}$$

where we recall that

$$\sigma_0 = \begin{bmatrix} 1 & 0 \\ 0 & 1 \end{bmatrix}, \quad \sigma_x = \begin{bmatrix} 0 & 1 \\ 1 & 0 \end{bmatrix}, \quad \sigma_y = \begin{bmatrix} 0 & -i \\ i & 0 \end{bmatrix} \quad \text{and} \quad \sigma_z = \begin{bmatrix} 1 & 0 \\ 0 & -1 \end{bmatrix}.$$

If we apply a Fourier transform in 2.3.31 from real to k-space, we arrive at

$$\begin{aligned} H(k) &= U + Te^{ik} + T^\dagger e^{-ik} = U + (T + T^\dagger)\cos k + i(T - T^\dagger)\sin k \\ &= t\sigma_x + \mu\cos k\sigma_x + \mu\sin k\sigma_y \\ &= h_x(k)\sigma_x + h_y(k)\sigma_y + h_z(k)\sigma_z = \mathbf{h}(k)\cdot\boldsymbol{\sigma} \end{aligned}$$

where in the last line we introduced

$$h_x(k) = t + \mu\cos k, \quad h_y(k) = \mu\sin k, \quad h_z(k) = 0. \tag{2.3.34}$$

Using anticommutation relations of the Pauli matrices it can be verified that $[H(k)]^2 = [E(k)]^2\sigma_0$ and we thus obtain the dispersion relations for the two bands

$$E_\pm(k) = \pm|t + \mu e^{-ik}| = \pm\sqrt{t^2 + \mu^2 + 2t\mu\cos(k)}. \tag{2.3.35}$$

We notice that for staggered hopping an energy gap of 2Δ, with

$$\Delta = \min E(k) = |t - \mu|, \tag{2.3.36}$$

separates the two bands (see fig. 2.9), and the system is an insulating phase. For $t = \mu$, on the other hand, the SSH model is in a conducting phase. The staggering of the

hopping amplitudes occurs naturally in many solid state systems, e.g., polyacetylene, by what is known as the Peierls instability [6]. As the gap due to the staggering of the hopping amplitudes opens, the energy of occupied states is lowered, while unoccupied states move to higher energies. Thus, the staggering is energetically favorable.

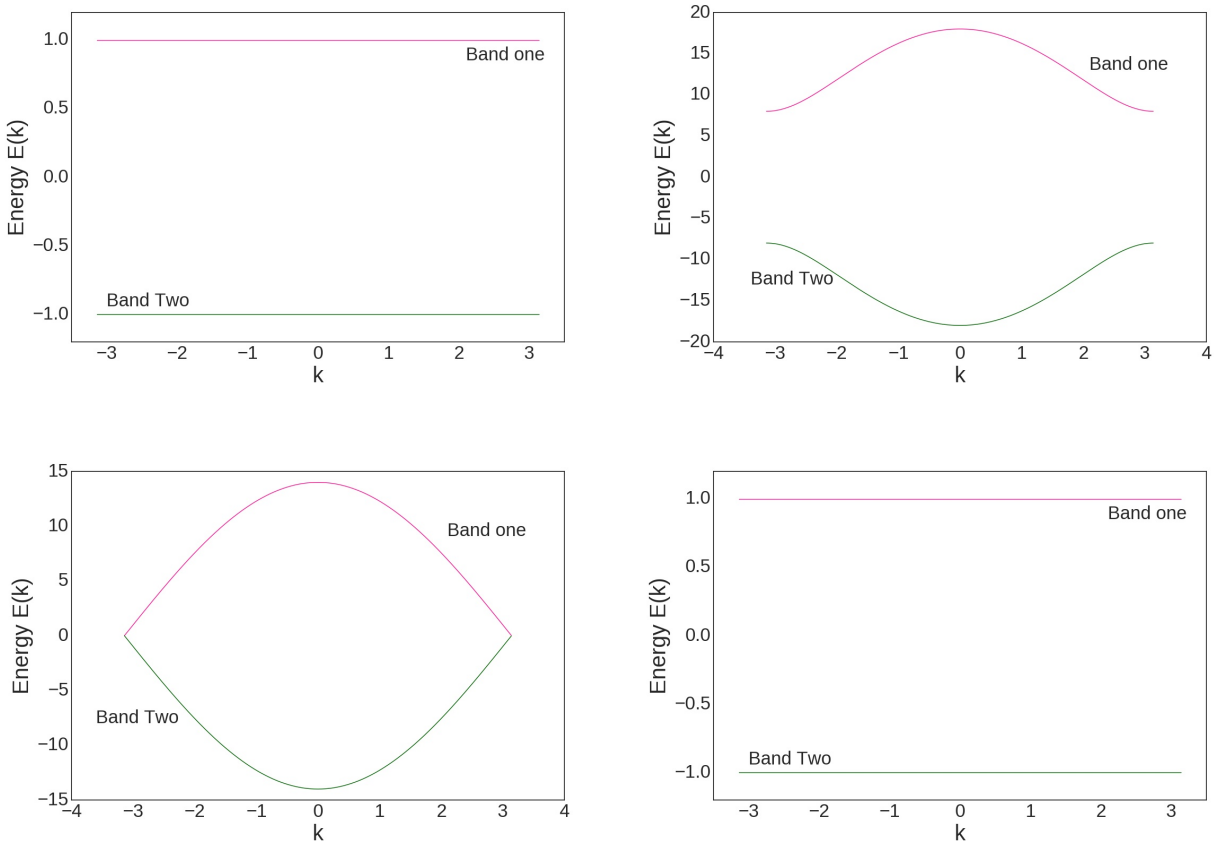

Figure 2.9: Dispersion relations of the SSH model that determines the energy level of each band. Values for hopping amplitudes are set according to: $\mu = 0$; $\mu = t$; $\mu < t$; $t = 0$.

2.3.1 Chiral symmetry

The Hamiltonian (2.3.29) describes a bipartite system: there are no transitions between sites within the same sublattice and we can define projectors in these sub-

lattices (say A and B) as

$$P_A = \sum_{r=2n} |r\rangle\langle r| \quad \text{and} \quad P_B = \sum_{r=2n+1} |r\rangle\langle r|. \tag{2.3.37}$$

The chiral symmetry is represented by the operator $\Sigma_z = P_A - P_B$: it is hermitean, unitary and local. There are no onsite terms in the Hamiltonian, so

$$\Sigma_z H \Sigma_z = -H$$

(anticommutation). A consequence of this chirallity is the symmetry of the spectrum: every eigenstate E has a partner $-E$, that is

$$H|\psi_n\rangle = E_n|\psi_n\rangle \longrightarrow H\Sigma_z|\psi_n\rangle = -\Sigma_z H|\psi_n\rangle = -\Sigma_z E_n|\psi_n\rangle = -E_n\Sigma_z|\psi_n\rangle \tag{2.3.38}$$

For any eigenstate with nonzero energy, flipping the sign of the wavefunction on the odd sites gives another eigenstate with opposite energy.

2.3.2 Bulk winding number

Let us consider the bulk Hamiltonian $H(k) = \mathbf{h}(k) \cdot \boldsymbol{\sigma}$. As k goes through the Brillouin Zone ($k = 0 \to 2\pi$), the tip of the vector $\mathbf{h}(k)$ runs through a closed path in the (h_x, h_y) plane. One can associate to this closed path a winding number ν, which counts how many times this path circles around the origin. Notice that in the insulating phase this path always avoids the origin because if there is a k at which $\mathbf{h} = 0$, the gap would close at this k, and we would not have an insulator. The chiral symmetry, on the other hand, ensures that the vector $\mathbf{h}(k)$ is restricted to lie on the XY plane.

To calculate this winding number consider a projection of the closed path to the unit circle. Recall that the winding number is a topological property which does not change under continuous deformations. One can then calculate the winding in terms of the unit vector

$$\tilde{\mathbf{h}}(k) = \mathbf{h}(k)/|\mathbf{h}(k)|$$

(see figure 2.10), by computing the area enclosed by $\tilde{\mathbf{h}(k)}$, and then dividing this area by the surface of the unit circle [6],

$$\nu = \frac{1}{2\pi} \int_{-\pi}^{\pi} dk \left(\tilde{\mathbf{h}}(k) \times \frac{\partial}{\partial k} \tilde{\mathbf{h}}(k) \right)_z . \tag{2.3.39}$$

Since the bulk Hamiltonian is off-diagonal,

$$H(k) = \begin{pmatrix} 0 & h(k) \\ h^*(k) & 0 \end{pmatrix}; \quad h(k) = h_x(k) - ih_y(k)$$

we can write the winding number as the following integral

$$\nu = \frac{1}{2i\pi} \int_{-\pi}^{\pi} \mathrm{d}k \frac{\mathrm{d}}{\mathrm{d}k} \log h(k). \tag{2.3.40}$$

One can readily compute the winding number for the SSH model in the insulating phase. It turns out to be 0 in cases the intracell hopping dominates over the intercell ($t > \mu$), and 1 in cases the intercell hopping dominates over the intracell ($t < \mu$). We say that the insulator is in the trivial phase if $\nu = 0$ and otherwise in a topological nontrivial phase, here characterized by $\nu = 1$.

Notice that there are two ways to change the winding number and get a topological transition: Either one has to deform the path through the origin in the (k_x, k_y)-plane, or one lifts the path out of the plane. In the first case one makes a transition through a metallic phase and in the second case one breaks the chiral symmetry.

We here close our introduction on Anderson localization and the SSH model as one example of a topological insulator. In the next chapter, we turn to the main system of interest for this thesis, the disordered SSH model.

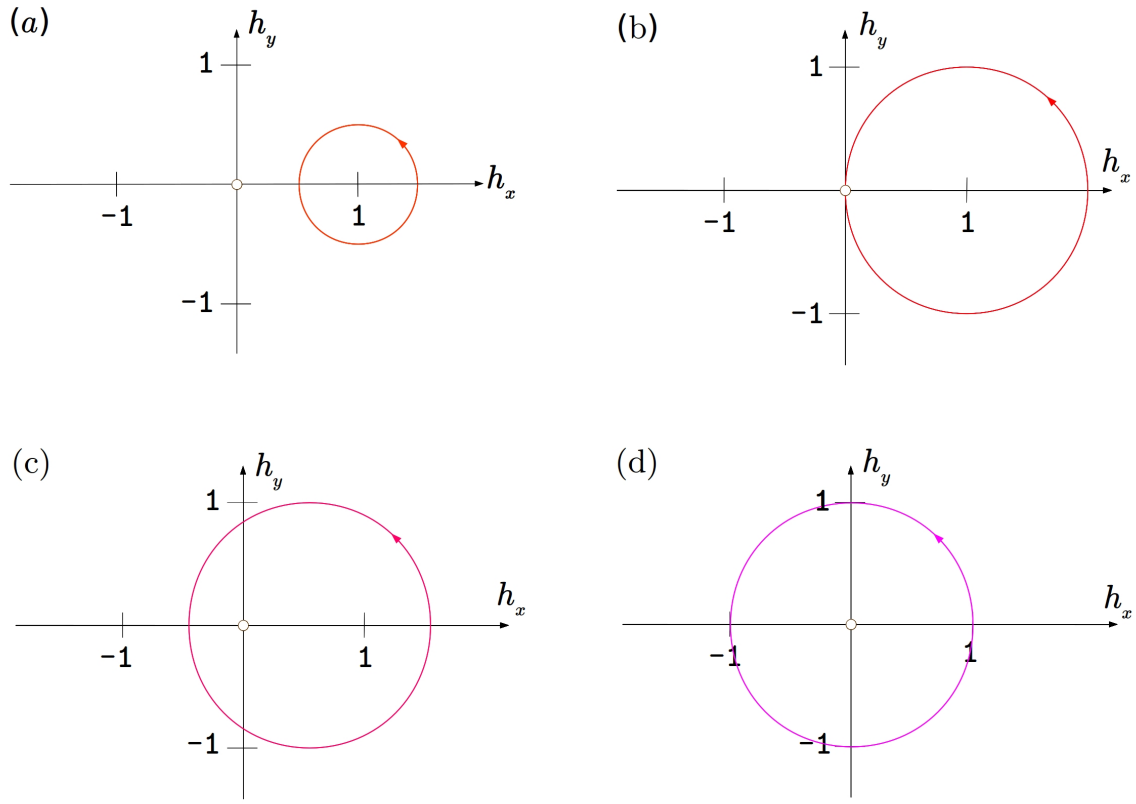

Figure 2.10: Winding number of the Bloch Hamiltonian of the SSH model. The loop is performed by the vector $h(k)$ on the plane (h_x, h_y), parametrized by: (a) $t = 1$, $\mu = 0.5$; (b) $t = 0.5$, $\mu = 0.5$; (c) $t = 0.4, \mu = 0.8$; (d) $t = 0.5$,$\mu = 0.5$ now closing the loop as $k \longrightarrow 2\pi$. The number of times that the origin is encircled by the loop, the topological invariant discontinuously changes, accompanied by a closing of the band gap.

Chapter 3

SDRG of a disordered SSH model

In this thesis we study the disordered SSH model as an example of a topologically nontrivial Anderson insulator. This chapter contains a study of how the single-parameter scaling of conventional Anderson insulators has to be generalized to obtain a complete picture once non-trivial topology comes into play.

In section 3.1 we introduce the model, which generalizes the SSH model already presented in chapter 2, to include disorder in form of random alternating hoppings in a way to keep the chiral symmetry. We then generalize the topological invariant to a disordered system, and derive in section 3.2 the second scaling parameter. The main ideas behind the SDRG are introduced in section 3.3, where we derive the decimation rules for the hoping terms in the SSH model. Also, we compute the second scaling parameter to the disordered chain in section 3.3.2. We conclude with a discussion of the two-parameter flow diagram in section 3.4.

3.1 The disordered SSH model

We consider a disordered single channel quantum wire with chiral symmetry, described by the Hamiltonian

$$H = \sum_{i,j=1}^{2L} c_i^\dagger T_{ij} c_j, \tag{3.1.1}$$

where $c_i^\dagger(c_j)$ is the canonical creation (annihilation) operator at site i and L is the physical length of the wire. The hopping amplitude has an alternating strength that

can be written as

$$T_{2i-1,2i} = T_{2i,2i-1} \equiv \mu_i \tag{3.1.2}$$

$$T_{2i+1,2i} = T_{2i,2i+1} \equiv t_i, \tag{3.1.3}$$

where t_i and μ_i are random variables with

$$\begin{aligned} \langle \mu_i \rangle = \mu, \quad \langle \mu_i \mu_j \rangle = v_\mu^2 \delta_{ij}, \\ \langle t_i \rangle = t, \quad \langle t_i t_j \rangle = v_t^2 \delta_{ij}. \end{aligned} \tag{3.1.4}$$

We will later consider

$$\begin{aligned} t_i = t v_i, \quad \mu_i = \mu v_i, \\ \langle v_i \rangle = 1, \quad \langle v_i v_j \rangle = v^2 \delta_{ij}. \end{aligned} \tag{3.1.5}$$

Rewriting the Hamiltonian 3.1.1 in matrix form, we have

$$H = \sum_{i,j=1}^{L} \begin{bmatrix} c_{i,+}^\dagger & c_{i,-} \end{bmatrix} \begin{bmatrix} 0 & \mu_i + t_i \hat{t}_a \\ \mu_i + t_i \hat{t}_a^{-1} & 0 \end{bmatrix} \begin{bmatrix} c_{i,+}^\dagger \\ c_{i,-} \end{bmatrix}, \tag{3.1.6}$$

where $\hat{t}$ is the single site translation operator.

3.2 Disordered system: topological invariant, two-parameter flow

The first step is to obtain the topological invariant χ for the disordered model. Let us recall the standard winding number construction for the clean system [25] previously mentioned. In the clean case, one can turn to the Fourier representation with a given wavenumber k such that the matrix elements are [17]:

$$h_{i,j}(k) = \delta_{ij}(\mu + te^{ik}),$$

and the topological number, introduced in 2.3.40,

$$\chi = \frac{1}{2\pi} \operatorname{Im} \int_0^{2\pi} dk tr[h^{-1}(k) \partial_k h(k)] = \Theta(|t| - |\mu|). \tag{3.2.7}$$

How can we generalize this number to a disordered system, i.e., without appealing to the k space? The answer comes as a trick: we consider a system with L unit cells

and periodic boundary conditions in a ring geometry ($i \equiv 2L + i$), and introduce by convenience the unit cell notation,

$$c_{2i} \longrightarrow c_{+,i} \qquad\qquad c_{2i-1} \longrightarrow c_{-,i}. \tag{3.2.8}$$

Through this ring, we insert a 'chiral flux' that affects the block matrices h as

$$\begin{aligned} h_{ij}(k) &= h_{ij}(k + \phi/L) \\ h^{\dagger}_{ij}(k) &= h^{\dagger}_{ij}(k - \phi/L). \end{aligned} \tag{3.2.9}$$

In other words, the non-unitary axial transformation,

$$T_{jk} \longmapsto T^{\phi}_{jk} \equiv T_{jk} \exp\left[-\frac{i\phi}{L}(j(-)^j + k(-)^k)\right], \tag{3.2.10}$$

explicitly changes the hopping as

$$\mu_j \longmapsto \mu^{\phi}_j \equiv \mu_j e^{i\frac{\phi}{L}}, \qquad\qquad t_j \longmapsto t^{\phi}_j \equiv t_j e^{-i\frac{\phi}{L}}. \tag{3.2.11}$$

The second step is to define the zero energy retarded Green function $G_\phi = (i0 - H^\phi)^{-1}$, and understand how it changes with the insertion of the chiral flux.

Considering first the translational invariant case, we notice that

$$\frac{1}{4\pi} \ln\left(\frac{\det(G_{2\pi})}{\det(G_0)}\right) = \frac{1}{4\pi}\int_0^{2\pi} d\varphi tr(\partial_\varphi \ln(G_\phi)) \tag{3.2.12}$$

$$= \frac{1}{4\pi}\sum_k \int_0^{2\pi} d\varphi tr\left[\partial_\varphi\left(\ln h(k + \varphi/L) + \ln h^{\dagger}(k - \varphi/L)\right)\right], \tag{3.2.13}$$

where in the last line we used the translational invariance. We then use the identity $\sum_k \int_0^{2\pi} d\varphi F(k + \varphi/L) = L \int dk F(k)$, to obtain

$$\frac{1}{4\pi} \ln\left(\frac{\det(G_{2\pi})}{\det(G_0)}\right) = \frac{i}{2\pi L} Im \sum_k \int_0^{2\pi} dk tr\left[\partial_k\left(\ln h(k)\right)\right],$$

which is exactly the winding earlier introduced in eq. 3.2.7. Then, we see that

$$\chi = \frac{1}{4\pi} \operatorname{Im} \ln\left[\frac{\det(G_{2\pi})}{\det(G_0)}\right]. \tag{3.2.14}$$

This equation represents the topological invariant in terms of a "spectral flow" [17]. As we earlier mentioned in section 2.2, this topological invariant becomes our

second scaling parameter. We then define the β function associated with each scaling parameter as

$$\beta_g(g,\chi) = \frac{d\ln g}{d\ln L} \quad \text{and} \quad \beta_\chi(g,\chi) = \frac{d\ln \chi}{d\ln L}. \tag{3.2.15}$$

Now we introduce the generating function [17]

$$\mathcal{F}(\varphi) = -\partial_\phi \langle \ln\det G_\phi\rangle|_{\phi=\varphi}. \tag{3.2.16}$$

Finally, the idea is to compute the two physical quantities of interest (that is, the two scaling parameters (g,χ)), from this generating function

$$g = -\partial_\varphi \mathcal{F}(\varphi)|_{\varphi=0} \quad \text{and} \quad \chi = \frac{1}{4\pi}\int_0^{2\pi} d\varphi\, \mathrm{Im}\,\mathcal{F}(\varphi), \tag{3.2.17}$$

and then to derive the flow equations using the SDRG rules. In the following section, we describe this procedure.

3.3 SDRG

Usually one uses the Strong Disorder Renormalization Group (SDRG) in the study of disordered systems. This method was introduced by C. Dasgupta and S.K. Ma in the 80's [23] and was further developed by Fisher [10] in a context of disordered spin chains. In this section, we describe the main RG-step in a SSH model of the previous sections, where disorder has been introduced by taken staggered amplitudes from some probability distribution. This step is the decimating procedure for hopping-terms and onsite energies from the Hamiltonian. Our discussion here is guided by the work in ref. [13].

3.3.1 The RG step: Decimating a hopping term

The basic idea behind a SDRG step, as in a normal RG step, is to successively integrate out high-energy modes and renormalize the remaining degrees of freedom (see figure 3.1). If the hopping terms are drawn from a random distribution, then there will be one bond with a much larger coupling than those in the rest of the system.

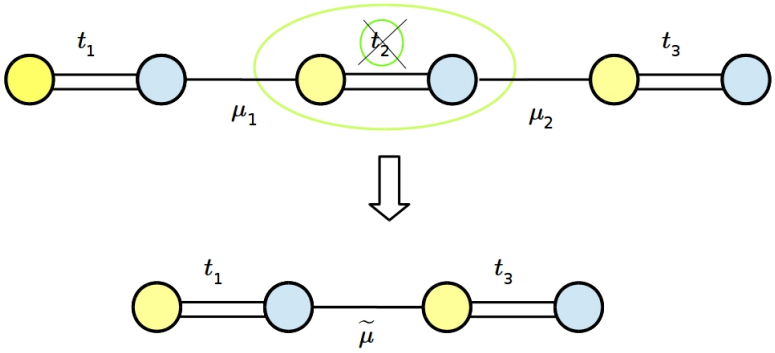

Figure 3.1: Scheme for the SDRG step.

We first locate this bond in the Hamiltonian 3.1.1 and name it as the cuttoff of our problem, that is $\Omega = \max\{|t_i|, |\mu_i|\}$. Let us consider, for example, the case where the largest coupling is $|t_2|$. In a language of perturbation theory, we can separate the Hamiltonian in two parts:

$$H = H_0 + H_1, \tag{3.3.18}$$

where we treat

$$H_0 = t_2 \hat{c}_2^\dagger \hat{c}_3 + \text{h.c.} \tag{3.3.19}$$

exactly, and

$$H_1 = \sum_{i\neq 2}^{N} t_i \hat{c}_{2i-1}^\dagger \hat{c}_{2i} + \sum_{i=1}^{N} \mu_i \hat{c}_{2i}^\dagger \hat{c}_{2i+1} + \text{h.c.} \tag{3.3.20}$$

in second order perturbation theory. The unperturbed Hamiltonian reads

$$H_0 = \begin{pmatrix} 0 & t_2 \\ t_2 & 0 \end{pmatrix}. \tag{3.3.21}$$

The eigen-energies are just $\lambda_\pm = \pm\sqrt{t_2^2} = \pm|t_2|$, with corresponding eigenvectors

$$|+\rangle = \frac{|1\rangle + |0\rangle}{\sqrt{2}} \tag{3.3.22}$$

$$|-\rangle = \frac{|1\rangle - |0\rangle}{\sqrt{2}}. \tag{3.3.23}$$

Treating H_1 perturbatively, the first order correction is zero and we should find the second order correction. Let's use $|1\rangle \equiv |1_k; 0\rangle$ to indicate a particle out of site

2 and $|0\rangle \equiv |0;\pm\rangle$ for when the particle is at the highest energy state. The effective hopping $\tilde{t}$ reads

$$\tilde{t_2} = \sum_{s=\pm} \frac{\langle 1_k;0|H_1|0;s\rangle\langle 0;s|H_1|1_l;0\rangle}{-\lambda_s}$$

$$\implies \quad \tilde{t_2} = \frac{\langle 1_k;0|H_1|0;+\rangle\langle 0;+|H_1|1_l;0\rangle}{-\lambda_+} + \frac{\langle 1_k;0|H_1|0;-\rangle\langle 0;-|H_1|1_l;0\rangle}{-\lambda_-}.$$

So we arrive at the renormalized hopping term $\tilde{t_2}$:

$$\tilde{t}_2 = -\frac{\mu_1\mu_3}{t_2}, \tag{3.3.24}$$

and in a similar way, the renormalized hopping $\tilde{\mu}$

$$\tilde{\mu}_2 = -\frac{t_1 t_3}{\mu_2}. \tag{3.3.25}$$

3.3.2 Back to generating function for disordered SSH model

With these preparation we now return to the calculation of the disorder averaged generating function $\mathcal{F}(\varphi)$ using the SDRG method. We eliminate sucessively largest energies until we arrive at a two site problem described by a single unit cell Hamiltonian, then use the generating function to this two-site problem. The relations for a single elimination step are exact transformations. We now rewrite our Hamilonian considering transformations in eq. 3.2.11,

$$H = \begin{bmatrix} 0 & (\mu e^{\frac{-i\phi}{L}} + te^{\frac{i\phi}{L}}) \\ (\mu e^{\frac{-i\phi}{L}} + te^{\frac{i\phi}{L}}) & i0 \end{bmatrix}$$

From the retarded Green's function, we have

$$G_\phi = \begin{bmatrix} i0 & -(\mu e^{\frac{-i\phi}{L}} + te^{\frac{i\phi}{L}}) \\ -(\mu e^{\frac{-i\phi}{L}} + te^{\frac{i\phi}{L}}) & i0 \end{bmatrix}^{-1} = -\begin{bmatrix} i0 & \frac{1}{\mu e^{\frac{-i\phi}{L}} + te^{\frac{i\phi}{L}}} \\ \frac{1}{\mu e^{\frac{-i\phi}{L}} + te^{\frac{i\phi}{L}}} & i0 \end{bmatrix} \tag{3.3.26}$$

Then we can compute the generating funcion as defined in 3.2.16

$$\mathcal{F}(\varphi) = -\partial_\phi \langle \ln \det G_\phi \rangle|_{\phi=\varphi} \tag{3.3.27}$$

$$= -\partial_\varphi \ln \left[\frac{1}{(\mu e^{\frac{-i\varphi}{L}} + te^{\frac{i\varphi}{L}})^2} \right] \tag{3.3.28}$$

$$= \partial_\varphi \ln \left[(\mu e^{\frac{-i\varphi}{L}} + te^{\frac{i\varphi}{L}})^2 \right] = 2\partial_\varphi \ln \left[(\mu e^{\frac{-i\varphi}{L}} + te^{\frac{i\varphi}{L}}) \right] \tag{3.3.29}$$

$$= 2\partial_\varphi \ln \left[te^{i\varphi/L} \left(1 + \frac{\mu}{t} e^{\frac{-2i\varphi}{L}} \right) \right] \tag{3.3.30}$$

$$= 2\partial_\varphi \ln t + 2\partial_\varphi \ln \left(e^{i\varphi/L} \right) + 2\partial_\varphi \ln \left(1 + \prod_{l=1}^{L} \frac{t_l}{\mu_l} e^{-2i\varphi/L} \right), \tag{3.3.31}$$

where we used that eqs. 3.3.25 are exact transformations. In order to check the consistency of our approach, let us recall the clean case, where we have $t_l = t$ and $\mu_l = \mu$. The above equation becomes

$$\mathcal{F}(\varphi) \approx 2\partial_\varphi \ln \left(1 + \left(\frac{t}{\mu} \right)^L e^{-2i\varphi/L} \right), \tag{3.3.32}$$

and from 3.2.17, we recover the topological winding number 2.3.40. Back to disorder, we obtain

$$\mathcal{F}(\varphi) = 2\partial_\varphi \ln \left(1 + \left(\frac{t}{\mu} \right)^L \frac{v_1 v_3 ... v_{2L-1}}{v_2 v_4 ... v_{2L}} e^{-2i\varphi/L} \right). \tag{3.3.33}$$

Following previous works [13], we consider a dimensionless scaling variable $\zeta_i = \ln(\Omega_0/v_i)$ in which

$$\zeta = -\ln(\overline{v}), \tag{3.3.34}$$

where $\overline{v} = \frac{v_1 v_3 ... v_{2L-1}}{v_2 v_4 ... v_{2L}}$ is a random walk in ζ_i-space. For large system sizes $L \gg 1$ is gaussian distributed by the central limit theorem,

$$P(\zeta) = \frac{1}{\sqrt{\pi v_\zeta^2}} e^{\frac{-\zeta^2}{v_\zeta^2}} \tag{3.3.35}$$

So, we can rewrite the topological invariant as

$$\chi = \int_0^{2\pi} \frac{d\varphi}{4\pi} \operatorname{Im} 2\partial_\varphi \ln \left[1 \mp \left(\frac{t}{\mu} \right)^L e^{\zeta} e^{2i\varphi/L} \right] = \Theta(L \ln(t/\mu) - 2\zeta), \tag{3.3.36}$$

and upon disorder average

$$\chi = \frac{1}{2} \left[1 - Erf \left(\frac{L}{v_\zeta \ln(\mu/t)} \right) \right]. \tag{3.3.37}$$

Notice that in the particle-hole symmetric point, $t = \mu$ is an unstable fixed point with $\chi = \frac{1}{2}$. On the other hand, the conductance will be

$$g = -\partial_\varphi \left[2\partial_\varphi \ln \left(1 + \left(\frac{t}{\mu}\right)^L \frac{v_1 v_3 ... v_{2L-1}}{v_2 v_4 ... v_{2L}} e^{-2i\varphi/L} \right) + \mathcal{O}(1/L) \right]_{\varphi=0}$$

$$\implies g = -\partial_\varphi \left[2\partial_\varphi \ln \left(1 + \left(\frac{t}{\mu}\right)^L 2e^{\zeta} e^{2i\varphi/L} \right) \right]_{\varphi=0}.$$

Now we can compute the conductance.

3.3.3 Exact results

From eq. 3.3.2 we obtain, for a single realization of disorder,

$$\begin{cases} g_\zeta = \dfrac{2}{\sinh^2(2\zeta - L\ln(t/\mu))}, & L = 4k \\ g_\zeta = \dfrac{2}{\cosh^2(2\zeta - L\ln(t/\mu))}, & L = 4k+2 \end{cases} \tag{3.3.38}$$

Upon disorder average, we obtain the average conductance:

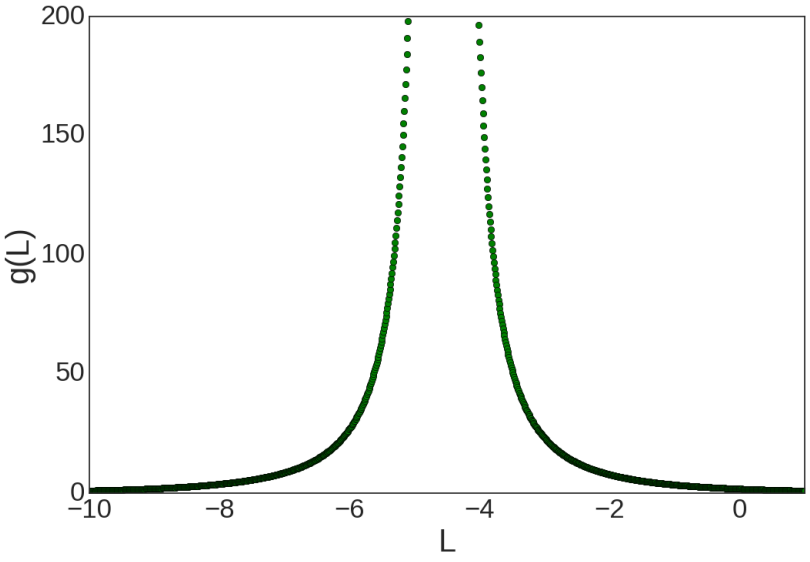

Figure 3.2: Illustraive plot for the conductance.

Typical vs. average conductance

Let us analyze the behavior of g in the limits of the system size L. From (3.3.38) we compute the distribution of conductance samples. Using the fact that

$$\sinh x = \frac{1-e^{-2x}}{2e^{-x}} \quad \text{and} \quad \cosh x = \frac{1+e^{-2x}}{2e^{-x}}, \tag{3.3.39}$$

and rewriting the argument as $\tilde{\zeta} = 2\left[\zeta - L\ln(t/\mu)\right]$, the conductance (one realization of disorder) reads

$$g_\zeta = \frac{16e^{-2\tilde{\zeta}}}{(1-e^{-2\tilde{\zeta}})^2}, \quad (L=4k), \qquad \text{and} \qquad g_\zeta = \frac{16e^{-2\tilde{\zeta}}}{(1+e^{-2\tilde{\zeta}})^2}, \quad (L=4k+2). \tag{3.3.40}$$

One can chose only one case, e.g. $L = 4k$, then the other will be analogous, so trough (3.3.35) yelds the typical conductance

$$\ln g_{\tilde{\zeta}} = \ln\left[\frac{16}{e^{2\tilde{\zeta}}(1-e^{-2\tilde{\zeta}})^2}\right] \quad \Longrightarrow \quad \ln g = \ln 16 - 2\langle\tilde{\zeta}\rangle - \left\langle 2\ln(1-e^{-2\tilde{\zeta}})\right\rangle.$$

Finally,

$$\ln g = \ln 16 - 4\langle[\zeta - L\ln(t/\mu)]\rangle - \left\langle 2\ln\left(1-e^{-4[\zeta-L\ln(t/\mu)]}\right)\right\rangle, \tag{3.3.41}$$

that lead us to the β-function defined in (3.2.15)

$$\beta_g = 4L\ln\left(\frac{t}{\mu}\right) - 8\left\langle\frac{L\ln(t/\mu)}{e^{4[\zeta-L\ln(t/\mu)]}-1}\right\rangle. \tag{3.3.42}$$

We also compute β_χ from (3.2.15) and (3.3.37), using the trick from the chain rule

$$\beta_\chi = \frac{d(\ln\chi)}{d\ln L} = \frac{dL}{d\ln L}\frac{d}{dL}(\ln\chi) = L\frac{d}{dL}(\ln\chi), \tag{3.3.43}$$

and then

$$\beta_\chi = L\frac{d}{dL}\ln\left\{\frac{1}{2}\left[1 - Erf\left(\frac{L}{v_\zeta\ln(\mu/t)}\right)\right]\right\} = \frac{4Lv_\zeta e^{\left[\frac{L}{v_\zeta}\ln\left(\frac{\mu}{t}\right)\right]^2}}{\sqrt{\pi}\ln(\mu/t)\left[Erf\left[\frac{L}{v_\zeta}\ln(\mu/t)\right]-1\right]}. \tag{3.3.44}$$

Since we are interested in the limit $L \to \infty$, we can use the following divergent asymptotic expansion

$$Erf(x) \approx 1 - e^{-x^2}(x\sqrt{\pi})^{-1}\left[1 - \frac{1}{2x^2} + ...\right],$$

and so

$$Erf\left[\frac{L}{v_\zeta}\ln\left(\frac{\mu}{t}\right)\right] \approx 1 - \frac{e^{-\left[\frac{L}{v_\zeta}\ln\left(\frac{\mu}{t}\right)\right]^2}}{\sqrt{\pi}\left(\frac{L}{v_\zeta}\ln(\mu/t)\right)}\left[1 - 2\left[\frac{L}{v_\zeta}\ln(\mu/t)\right]^{-2} + ...\right]. \quad (3.3.45)$$

After some algebra and considering only the first two terms of the expansion, the eq. (3.3.44) becomes

$$\beta_\chi \approx \left[\frac{2v_\zeta}{\sqrt{\pi}\ln\left(\frac{\mu}{t}\right)}\right]^2\left[1 - \frac{{v_\zeta}^2}{2L^2\ln^2\left(\frac{\mu}{t}\right)}\right] \quad (3.3.46)$$

3.4 Discussion

In this first part, we have studied a disordered one-dimensional wire with chiral symmetry. We have shown how the single parameter scaling hypothesis by the so called "gang of four" has to be generalized to account for topologically nontrivial phases. While topologically trivial systems follow single parameter flow, fully characterized by the conductance, the topological index enters as second relevant parameter in systems allowing for topologically non-trivial insulating phases. Specifically, we discussed how the winding number can be generalized from translational invariant to disordered systems.

We obtained using the SDRG procedure, the flow of the two scaling parameters and then analyzed the change of average winding in a disordered SSH chain. We found a phase diagram summarized in fig. 3.3. Generically, the system flows to one of two possible Anderson insulating phases characterized by windings $0, 1$.

The disordered SSH chain has been previously analyzed in the limit of a large number $N \gg 1$ of channels (i.e., quasi one-dimensional rather than one-dimensional system) in ref. [17]. We obtained in the case $N = 1$, qualitatively, similar results (same phase diagram, as expected), though scaling functions differ in detail. While the field theory approach is rather involved and requires knowledge of advanced methods, the SDRG approach, on the other hand, is rather simple. There however, only the flow of the conductance was studied and we here presented how to complete the picture taking into account the winding number.

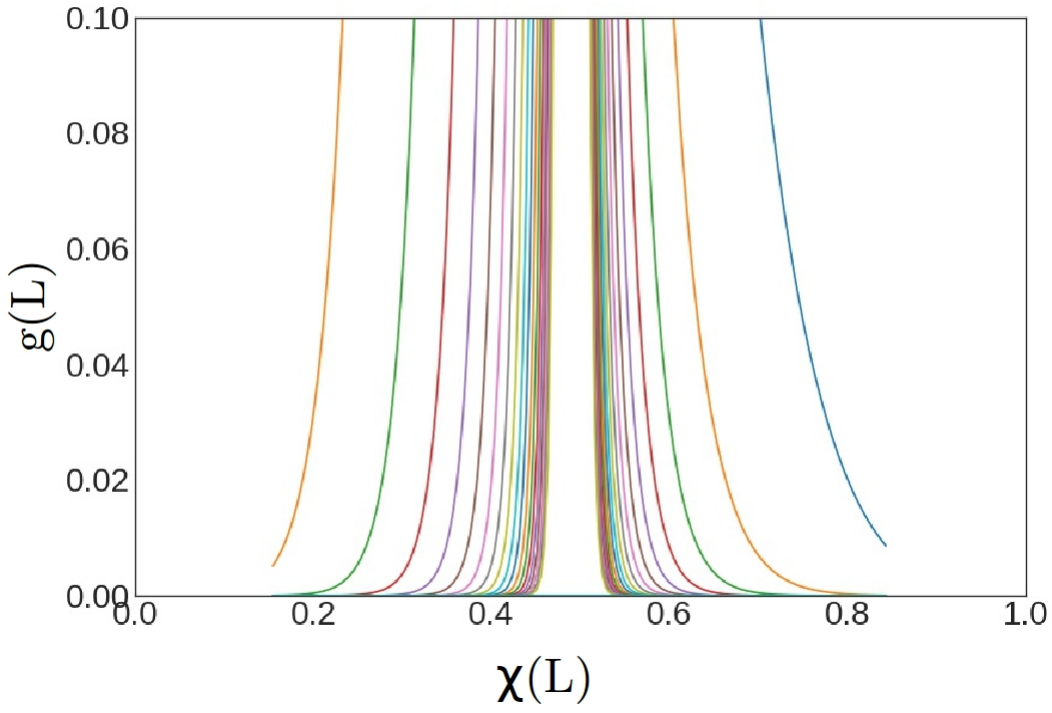

Figure 3.3: Two parameter flow ($\chi(L)$,$\beta(L)$) diagram. Notice that when the system is fine tuned to the critical state $\chi = 1/2$, the topological number does not flow.

Here, we close the first part. In the next chapter, we present a different perspective and look at the $N = 3$ connected channels, preparing the required parameters to build a supervised Machine Learning algorithm.

Part II

Machine Learning

Chapter 4

Special case: $N = 3$ connected chains

In this second part, we aim to understand what a Machine Learning (ML) algorithm can say about the topological phases of a finite disordered system.

In the first part, we argued that the field theory description for N connected chains is not applicable in the case where $N = 1$. In the construction of this field theory, the topological parameter is obtained by a perturbative self-consistent Born approximation (SCBA). Along in ref. [17], they provided a numerical verification of this approach, that worked well when $N = 3$ wires. They also obtained a phase diagram in this particular case.

The idea in this second part is to reproduce the same phase diagram from a Machine Learning algorithm. When one uses this approach, the data generated is supposed to have a Hamiltonian (in the momentum-space representation) and corresponding topological number. Here is useful to compute the topological number in the real space.

In this chapter, we aim to analytically obtain the self-energy correction to compute the topological invariant for $N = 1$ and $N = 3$ disordered chains. Our starting point in section 4.1 is the self-consistent equation that defines the correction. We finally arrive in the topological invariant in section 4.2.

4.1 SCBA

It is known that an analytical approach for disordered topological insulators consists of the disordered averaged self-energy Σ using the Self-Consistent Born Approximation (SCBA) [26]. This approach is useful to our problem because a solution in low-energy approximation for the self-energy is momentum-independent.

$$\Sigma \approx -g \int \frac{d^d p}{(2\pi)^d} \frac{1}{p^2 + r - \Sigma}. \tag{4.1.1}$$

The above equation is "self-consistent" because the self-energies appears recursively on the right-hand side of the equation. Using this approximation, we can include the vertex corrections. The iteration generates an expansion in terms of the interaction and the Green's function will be a self-consistent solution of the Dyson equation.

In our model, we assume from symmetry arguments, that Σ can be expanded as $\Sigma_0\tau_0 + \Sigma_z\tau_z$ with

$$\Sigma_0 = \begin{pmatrix} 1 & 0 \\ 0 & 1 \end{pmatrix}, \quad \Sigma_z = \begin{pmatrix} 1 & 0 \\ 0 & -1 \end{pmatrix},$$

and from [26], we write this correction as

$$\Sigma = \sum_{d=1}^{6} \frac{W_d^2}{12} \sum_{k \in BZ} (\sigma\tau)_d \frac{1}{i\delta - H_0(k) - \Sigma} (\sigma\tau)_d, \tag{4.1.2}$$

where BZ means a summation over the Brillouin zone and $H_0(k)$ is the SSH hamiltonian already presented in 3.1.1. We have

$$\Sigma_0\tau_0 + \Sigma_z\tau_z = \frac{w^2}{2\pi} \int_{-\pi}^{\pi} dk \cdot \sigma_x \frac{1}{[i0 - H_0(\vec{\mathbf{k}}) - (\Sigma_0\tau_0 + \Sigma_z\tau_z)]} \sigma_x. \tag{4.1.3}$$

The disordered averaged propagator features renormalized mass and chemical potential as

$$\bar{m} = m_0 + \mathrm{Re}\,\Sigma_z \tag{4.1.4}$$

$$\bar{\mu} = \mu - \mathrm{Re}\,\Sigma_z. \tag{4.1.5}$$

The left side of (4.1.3) is just

$$\Sigma_0 \begin{pmatrix} 1 & 0 \\ 0 & 1 \end{pmatrix} + \Sigma_z \begin{pmatrix} 1 & 0 \\ 0 & -1 \end{pmatrix} = \begin{pmatrix} \Sigma_0 + \Sigma_z & 0 \\ 0 & \Sigma_0 - \Sigma_z \end{pmatrix}.$$

Let us denote as I the integral on the right side of 4.1.3, with the respective terms,

$$I = \frac{w^2}{2\pi}\int_{-\pi}^{\pi} dk \begin{pmatrix} 0 & 1 \\ 1 & 0 \end{pmatrix} \begin{bmatrix} i\delta - (\Sigma_0 + \Sigma_z) & -(\mu + te^{ik}) \\ -(\mu + te^{-ik}) & i\delta - (\Sigma_0 - \Sigma_z) \end{bmatrix}^{-1} \begin{pmatrix} 0 & 1 \\ 1 & 0 \end{pmatrix}$$

$$\implies \quad I = \frac{w^2}{2\pi}\int_{-\pi}^{\pi} dk \frac{1}{\Delta} \begin{pmatrix} 0 & 1 \\ 1 & 0 \end{pmatrix} \begin{bmatrix} (i\delta - \Sigma_0) + \Sigma_z & \mu + te^{ik} \\ \mu + te^{-ik} & (i\delta - \Sigma_0) - \Sigma_z \end{bmatrix} \begin{pmatrix} 0 & 1 \\ 1 & 0 \end{pmatrix}$$

$$\implies \quad I = \frac{w^2}{2\pi}\int_{-\pi}^{\pi} dk \frac{1}{\Delta} \begin{bmatrix} (i\delta - \Sigma_0) - \Sigma_z & \mu + te^{-ik} \\ \mu + te^{ik} & (i\delta - \Sigma_0) + \Sigma_z \end{bmatrix}, \tag{4.1.6}$$

where $\Delta = [(i\delta - \Sigma_0)^2 - \Sigma_z^2 - (\mu + te^{-ik})(\mu + te^{ik})]$. From now, we consider $\Sigma_z = 0$ and $i\delta \to 0$, that lead us to

$$\begin{pmatrix} \Sigma_0 & 0 \\ 0 & \Sigma_0 \end{pmatrix} = \frac{w^2}{2\pi}\int_{-\pi}^{\pi} dk \frac{1}{\Delta} \begin{bmatrix} -\Sigma_0 & \mu + te^{-ik} \\ \mu + te^{ik} & -\Sigma_0 \end{bmatrix}, \tag{4.1.7}$$

where now $\Delta = \Sigma_0^2 - (\mu^2 + t^2 + 2t\mu\cos k)$. Finally,

$$\Sigma_0 = -\frac{w^2}{2\pi}\int_{-\pi}^{\pi} dk \frac{\Sigma_0}{\Sigma_0^2 - (\mu^2 + t^2 + 2t\mu\cos k)}. \tag{4.1.8}$$

This is clearly a trigonometric contour integral, so we solve it first locating the poles inside the contour, finding the residues at these poles and then apply the residue theorem. The limits of integration are finite, which allows us to change the variables from k to $z = \mathrm{e}^{ik}$, with $0 \leqslant k \leqslant 2\pi$. Denoting the integral as I_2, we have

$$I_2 = -2i\int_0^{2\pi} \frac{dz}{2az + z^2 + 1}, \tag{4.1.9}$$

where $a = \frac{\mu^2 + t^2 - \Sigma_0^2}{2t\mu}$. The denominator can be written as

$$2az + z^2 + 1 = (z - r_1)(z - r_2), \quad r_1 + r_2 = -2a \quad \text{and} \quad r_1 r_2 = 1. \tag{4.1.10}$$

The residue theorem states that for any analytic function $f(z)$ with a pole at z_0

$$\oint_{\Gamma[z_0]} f(z)dz = \pm 2i\pi \mathrm{Res}[f(z)]_{z=z_0} \tag{4.1.11}$$

where $\Gamma[z_0]$ is an infinitesimal loop around z_0. The sign plus (minus) indicates if the loop goes counterclockwise (clockwise). With this, and considering the pole r_1 inside the contour, we have

$$I_2 = 2\pi i \mathrm{Res}_{r_1}\left[\frac{1}{(z-r_1)(z-r_2)}\right] = 4\pi \lim_{z\to r_1}\left[\frac{(z-r_1)}{(z-r_1)(z-r_2)}\right] = \frac{4\pi}{(r_1-r_2)}.$$

Since $r_1 = -a+\sqrt{a^2-1}$ and $r_2 = -a-\sqrt{a^2-1}$, the integral is just

$$I_2 = \frac{2\pi}{\sqrt{a^2-1}}. \tag{4.1.12}$$

And now we back to eq. (4.1.8),

$$1 = \frac{-w^2}{2\pi}\frac{(-2\pi)}{\sqrt{(\mu^2+t^2-\Sigma_0^2)^2-(2t\mu)^2}}$$

$$w^2 = \sqrt{(\mu^2+t^2-\Sigma_0^2)^2-(2t\mu)^2} \quad\Longrightarrow\quad w^4+(2\mu t)^2 = (\mu^2+t^2-\Sigma_0^2)^2$$

$$\Longrightarrow\quad \Sigma_0 = \left[\mu^2+t^2-\sqrt{w^4+(2t\mu)^2}\right]^{1/2}, \tag{4.1.13}$$

which is the solution for the self-energy.

4.2 Topological invariant in a disordered system

We now compute the topological invariant n considering the self-energy correction,

$$n = \frac{1}{4i\pi}\int_{-\pi}^{\pi} dk\,\mathrm{tr}(\sigma_z G\partial_k G^{-1}), \tag{4.2.14}$$

where the Green function G contains Σ,

$$G = -(H_0+\Sigma)^{-1} = -\begin{pmatrix} \Sigma_0 & \mu+te^{ik} \\ \mu+te^{-ik} & \Sigma_0 \end{pmatrix}^{-1},$$

$$\Longrightarrow\quad G = -\frac{1}{\Omega}\begin{pmatrix} \Sigma_0 & -(\mu+te^{ik}) \\ -(\mu+te^{-ik}) & \Sigma_0 \end{pmatrix}, \tag{4.2.15}$$

where

$$\Omega = \Sigma_0^2 - (\mu+te^{ik})(\mu+te^{-ik}). \tag{4.2.16}$$

The matrix product on the integral is just

$$\sigma_z \cdot G = -\frac{1}{\Omega}\begin{pmatrix} 1 & 0 \\ 0 & -1 \end{pmatrix}\begin{pmatrix} \Sigma_0 & -(\mu + te^{ik}) \\ -(\mu + te^{-ik}) & \Sigma_0 \end{pmatrix} = -\frac{1}{\Omega}\begin{pmatrix} \Sigma_0 & -(\mu + te^{ik}) \\ (\mu + te^{-ik}) & -\Sigma_0 \end{pmatrix}$$

Introducing this matrix above in (4.2.14):

$$n = \frac{1}{4i\pi}\int_{-\pi}^{\pi} dk \,\mathrm{tr}\left[\frac{1}{\Omega}\begin{pmatrix} \Sigma_0 & -\mu - te^{ik} \\ \mu + te^{-ik} & -\Sigma_0 \end{pmatrix}\begin{pmatrix} 0 & ite^{ik} \\ -ite^{-ik} & 0 \end{pmatrix}\right] \tag{4.2.17}$$

$$\implies \quad n = \frac{1}{4i\pi}\int_{-\pi}^{\pi} dk \,\mathrm{tr}\left\{\frac{1}{\Omega}\begin{pmatrix} ite^{-ik}(\mu + te^{ik}) & -it\Sigma_0 e^{ik} \\ it\Sigma_0 e^{-ik} & ite^{ik}(\mu + te^{-ik}) \end{pmatrix}\right\} \tag{4.2.18}$$

$$\implies \quad n = \frac{i}{4i\pi}\int_{-\pi}^{\pi} dk \left[\frac{te^{-ik}(\mu + te^{ik}) + te^{ik}(\mu + te^{-ik})}{\Sigma_0^2 - \mu^2 - t^2 - t\mu(e^{ik} + e^{-ik})}\right] \tag{4.2.19}$$

The numerator can be analyzed as

$$t\mu e^{-ik} + t^2 + t\mu e^{ik} + t^2 = 2t^2 + t\mu(e^{ik} + e^{-ik})$$

and dividing this integrand by $t\mu$, we obtain

$$n = \frac{i}{4i\pi}\int_{-\pi}^{\pi} dk \left[\frac{\frac{2t}{\mu} + (e^{ik} + e^{-ik})}{\left(\frac{\Sigma_0^2 - t^2 - \mu^2}{t\mu}\right) - (e^{ik} + e^{-ik})}\right] \tag{4.2.20}$$

This is another contour integral that can be solved as before, changing the variables to $z = e^{ik}$ and $dk = \frac{dz}{iz}$:

$$n = \frac{i}{4i\pi}\int_0^{2\pi} \frac{dz}{iz}\left[\frac{\frac{2t}{\mu} + (z + z^{-1})}{2a - (z + z^{-1})}\right] = \frac{-i}{4\pi}\int_0^{2\pi} dz \frac{bz + z^2 + 1}{z(2a - z^2 - 1)}, \tag{4.2.21}$$

with

$$2a = \left(\frac{\Sigma_0^2 - t^2 - \mu^2}{t\mu}\right) \quad \text{and} \quad b = \frac{2t}{\mu}. \tag{4.2.22}$$

The poles of the function are $z_0 = 0, z_1 = a - \sqrt{a^2 - 1}$ and $z_2 = a + \sqrt{a^2 - 1}$. This implies that the residues are

$$\mathrm{Res}_{z_0} = \lim_{z \to 0}\left[\left(\frac{bz + z^2 + 1}{2az^2 - z^3 - z}\right)(z - 0)\right] = -1;$$

$$\mathrm{Res}_{z_1} = \lim_{z\to z_1}\left[\left(\frac{bz+z^2+1}{(z-z_1)(z-z_2)}\right)(z-z_1)\right] = \frac{bz_1+z_1^2+1}{z_1-z_2};$$

$$\mathrm{Res}_{z_2} = \lim_{z\to z_2}\left[\left(\frac{bz+z^2+1}{(z-z_1)(z-z_2)}\right)(z-z_2)\right] = \frac{bz_2+z_2^2+1}{z_2-z_1}.$$

Finally, the integral reads

$$I_3 = 2i\pi\left[-1+\frac{b(z_1-z_2)+z_1^2-z_2^2}{z_1-z_2}\right]$$

$$I_3 = 2i\pi\left[-1+\frac{b(a-\sqrt{a^2-1}-(a+\sqrt{a^2-1}))+(a-\sqrt{a^2-1})^2+(a+\sqrt{a^2-1})^2+2}{(a-\sqrt{a^2-1})-(a+\sqrt{a^2-1})}\right]$$

$$\implies \quad I_3 = 2i\pi(b+2a-1) \tag{4.2.23}$$

and so the invariant takes the form

$$n = \frac{1}{2}\left(\frac{2t}{\mu}+\frac{\Sigma_0^2-t^2-\mu^2}{t\mu}-1\right). \tag{4.2.24}$$

Putting (4.1.13) into the above equation, we obtain the topological invariant in terms of the disorder avegare and the self-energy Σ,

$$n = \frac{1}{2}\left(\frac{2t}{\mu}-\frac{\sqrt{w^4+(2t\mu)^2}}{t\mu}-1\right), \tag{4.2.25}$$

or in its simplified form

$$n = \frac{t}{\mu}-\left(\frac{1}{2}+\sqrt{\frac{w^4}{(2t\mu)^2}+1}\right).$$

In the limit of weak disorder, we have $|t-\mu| \ll w \ll t$.

4.3 Self-energies for $N = 3$ chains

Let us consider a system with N chains of length L described by the Hamiltonian

$$H = \sum_l\left[C_l^\dagger\left((\mu+t)+(\mu-t)\hat{P}\right)\right]C_{l+1} + C_l^\dagger\hat{V}_l C_{l+1} + h.c., \tag{4.3.26}$$

where $C_l = c_{l,j}$ is the vector of fermion creation operators, the chain index is $j = 1, ..., N$, $l = 1, ..., L$ labels the chain sites, $\hat{P}c_{l,j} = (-)^l c_{l,j}$ is a parity operator, and the matrix $\hat{V}_l$ is a random inter-chain hopping, that has Gaussian distribution W^2/N. Without disorder, the winding number is defined and calculated as in the normal SSH chain. In this case, we use the same strategy as before to find the self-energies correction. We begin start rewriting the Hamiltonian ($N = 3$) as

$$\hat{H} = \sum_{l=1}^{L} \Big\{ c_{l,1}^\dagger \left[(\mu + t) + (\mu - t)(-)^l \right] c_{l+1,1} + c_{l,2}^\dagger \left[(\mu + t) + (\mu - t)(-)^l \right] c_{l+1,2} + \\ + c_{l,3}^\dagger \left[(\mu + t) + (\mu - t)(-)^l \right] c_{l+1,3} \Big\},$$

or in matrix form,

$$H = \begin{bmatrix} C_I^\dagger & C_{II}^\dagger & C_{III}^\dagger \end{bmatrix} \begin{bmatrix} \tilde{H}_I & 0 & 0 \\ 0 & \tilde{H}_{II} & 0 \\ 0 & 0 & \tilde{H}_{III} \end{bmatrix} \begin{bmatrix} C_I \\ C_{II} \\ C_{III} \end{bmatrix}, \tag{4.3.27}$$

where the index $i = I, II, III$ labels each chain and in the momentum space it can be written as bloch matrices 2×2, remaining as in (3.1.6) with $h_\pm(k) = \mu + te^{\pm ik}$. We then write the full shape of the hamiltonian as $\tilde{H}_i \otimes \mathbb{I}$, where $\mathbb{I}$ is the identity matrix of order $3L \times 3L$. Also,

$$C^\dagger = \begin{bmatrix} (c_{1,1}^\dagger & c_{2,1}^\dagger & ... & c_{L,1}^\dagger)_I & (c_{1,2}^\dagger & c_{2,2}^\dagger & ... & c_{L,2}^\dagger)_{II} & (c_{1,3}^\dagger & c_{2,3}^\dagger & ... & c_{L,3}^\dagger)_{III} \end{bmatrix}.$$

This means that is posible to write the self-energy equations as we did before, now taking into account that the Hamiltonian is a $(3L \times 3L)$ matrix, which means that a factor of 3 proportional to the number of chains must appear. Eq. (4.1.8) after symmetry considerations will be

$$\Sigma_0(\sigma_x \otimes \mathbb{I}) = \frac{\omega^2}{2\pi} \int_{-\pi}^{\pi} dk (\sigma_0 \otimes \mathbb{I}) \cdot \frac{1}{[(-\tilde{H}(\vec{k}) \otimes \mathbb{I}) - \Sigma_0(\sigma_x \otimes \mathbb{I})]} \cdot (\sigma_0 \otimes \mathbb{I})$$

$$\implies \Sigma_0(\sigma_x \otimes \mathbb{I}) = \frac{\omega^2}{2\pi} \int_{-\pi}^{\pi} dk (\sigma_0 \otimes \mathbb{I}) \cdot \frac{1}{-[(\tilde{H}(\vec{k}) + \Sigma_0\sigma_x) \otimes \mathbb{I})]} \cdot (\sigma_0 \otimes \mathbb{I}) \tag{4.3.28}$$

and the procedure is the same as we did before. In the limit of small disorder, we again have that $|t - \mu| \ll w \ll t$, and we write the self-energies as

$$w^2 = \sqrt{(\mu^2 + t^2 - \Sigma_0^2)^2 - (2t\mu)^2}$$

$$w^2 = \sqrt{(\mu^2 + t^2 - \Sigma_0^2)^2 - (2t\mu)^2} \quad \Longrightarrow \quad w^2 + (2\mu t)^2 = (\mu^2 + t^2 - \Sigma_0^2)^2$$

$$\therefore \quad \Sigma_0 = \left[\mu^2 + t^2 - \sqrt{w^4 + (2t\mu)^2}\right]^{1/2}, \tag{4.3.29}$$

We introduce a gaussian disorder of type w^2/N [17]. With this argument, we finally arrive at the topological number (analougously to the previous case)

$$n = \frac{3}{2}\left(\frac{2t}{\mu} - \frac{\sqrt{w^4 + (2t\mu)^2}}{t\mu} - 1\right). \tag{4.3.30}$$

Comparing this equation with 4.2, the difference is in a factor of 3. In the general case, where all chains are connected, we have an N factor. That is, the topological invariant becomes

$$n = \frac{N}{2}\left(\frac{2t}{\mu} - \frac{\sqrt{w^4 + (2t\mu)^2}}{t\mu} - 1\right). \tag{4.3.31}$$

We will use the result in eq. 4.3.30 in the generation of the datasets.

This particular case of $N = 3$ chains is interesting since its phase diagram was already presented in ref. [31], so we can compare if the ML algorithm is able to make the right classification. Fig. 4.1 shows this diagram.

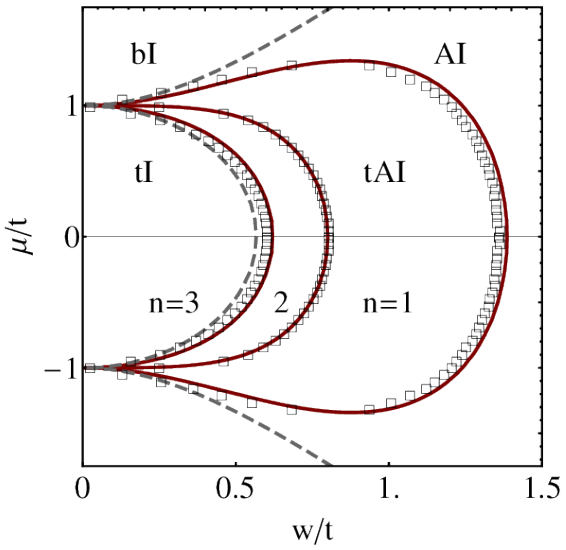

Figure 4.1: Phase diagram of the A-III class 3-channel disordered wire. Taken from [31].

Chapter 5

Machine Learning

It is very notorious that machines are increasingly influencing everyday decision-making: from web search results to spam filters, from suggestions on streaming media platforms to friends in social networks. This is possible due to developments in the field of Artificial Intelligence (AI) over the last decades. Machine Learning (ML) is a sub-field of AI that combines Statistics and Computer Science to extract knowledge from data, also known as predictive analysis or statistical Learning [29]. It has also a range of scientific applications like helping to discover distant planets and new particles or providing personalized cancer treatments .

In this chapter, we answer the question of how ML can be useful in the problem of classifying topological phases from data in the real space. We give a brief introduction about ML and Neural Networks (NN) in section 5.1, and detail the process of data generation for a topological insulator, with and without disorder, in section 5.1.1. Finally, in 5.2, some preliminary results are presented.

5.1 Brief introduction to ML

We classify machine learning systems in supervised, unsupervised, semi-supervised and reinforcement learning, according to the type and amount of supervision they get during training. The most used categories are the first two.

If a ML algorithm make predictions (outputs) from known data (inputs), we label it as a supervised algorithm. It can decide to which classes a given new input belongs

to, according with the training set of data. On the other hand, unsupervised learning occurs if the prediction is made only with the input data known (no output is given): the learner receives only unlabeled data and there are only inputs. Unsupervised algorithms are harder to implement.

Every problem requires a good knowledge of the dataset. The first step for build a ML algorithm is a good knowledge of the data you're working with and how it relates the tasks you want to solve. We chose to implement a supervised algorithm, but not discarding the idea of trying an unsupervised model in the future (in fact, ref. [36] shows an example of such implementation in the classification of exotic phases of matter).

5.1.1 Neural Networks

The process of building a NN consists of 4 steps: collect data, design features (features are those defining characteristics of a given dataset that allow for optimal learning [37]), train network and test network.

The basic unit in a NN is a neuron (in reference to the human brain. A neuron receives the input data and comput the output. Perceptrons are considered the simplest type of neurons, such they can process an input by computing a scalar product with a given weight and feeding the results in terms of a Θ function:

$$a(z) = \Theta(\mathbf{x} \cdot \mathbf{w} - b) = \Theta(z), \tag{5.1.1}$$

where a is the activation function, z is the weighted input, $\mathbf{x}$ is the input, $\mathbf{w}$ the weght vector and b a bias. In our model, we used the sigmoid as the activation function.

Among the many classes of NN, we chose by simplicity to use a Feedforward Neural Network (FNN). In this type of network, the information moves in only one direction (forward) from the input nodes trough the hidden layers/output nodes. We first perform the trivial topological insulator (SSH without disorder) in a few experiments, and later use the model for $N = 3$ connected chains presented in 4 to illustrate the non-trivial insulator, repeating the same procedure. The 4 steps in our experiments are: Creating datasets, which consists of generating Hamiltonians

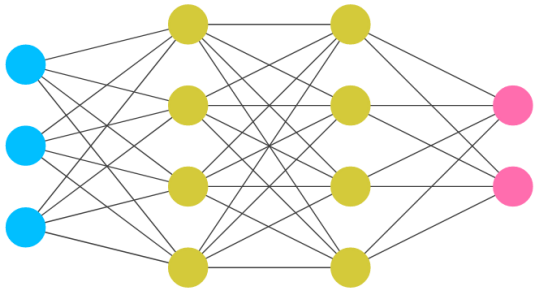

Figure 5.1: The layers in a neural network are in general structures where all neurons are connected to each other.

and Winding numbers and splitting them into training, testing and validation subsets; Training the eigenvectors in the real space, which consists of implement in a Feedforward neural network; and test the model to take the its accuracy.

5.2 Data generation

Our input labels are Hamiltonians H_i. In general, these Hamiltonians take a representation in the momentum space [35], that is $H = H(k)$. The targets are the corresponding topological invariants W_i. Guided by an approach made by Holanda and Rufo [34], our Hamiltonians are in the real space.

We generate a grid with 500 Hamiltonians that has periodic boundary conditions distributed in the parameter space μ-t, in order to recover the phase diagram in this space. Each Lattice had 30 unit cells. A plot for the spectrum is shown in fig. 5.2. We set $t = 1$.

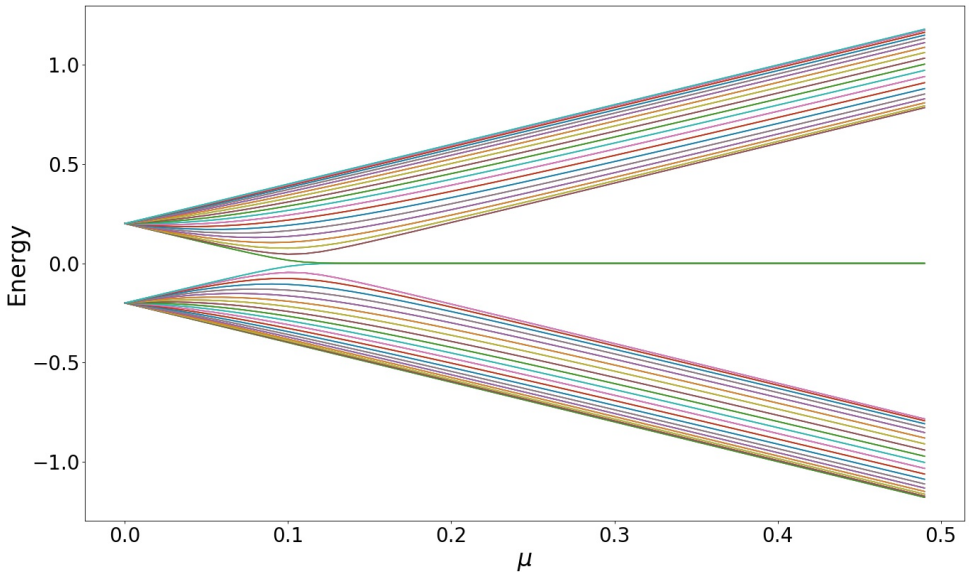

Figure 5.2: Variation of the energy E vs. hopping μ in the clean case. We set $t = 0.5$

In the disordered case, we generated a grid also with 500 Hamiltonians and periodic boundary conditions. An idea of how disorder can affect the energy spectrum is shown in fig. 5.3, in which we used $t = 0.5$ and a disorder of magnitude $V_0 = 0.8$.

We created a matrix of features and targets of variables. There were some columns that should be excluded from the analysis for not being usefull at all (this data cleaning process is usually boring). We used 80% of the dataset for training, 10% for test and 10% for validation.

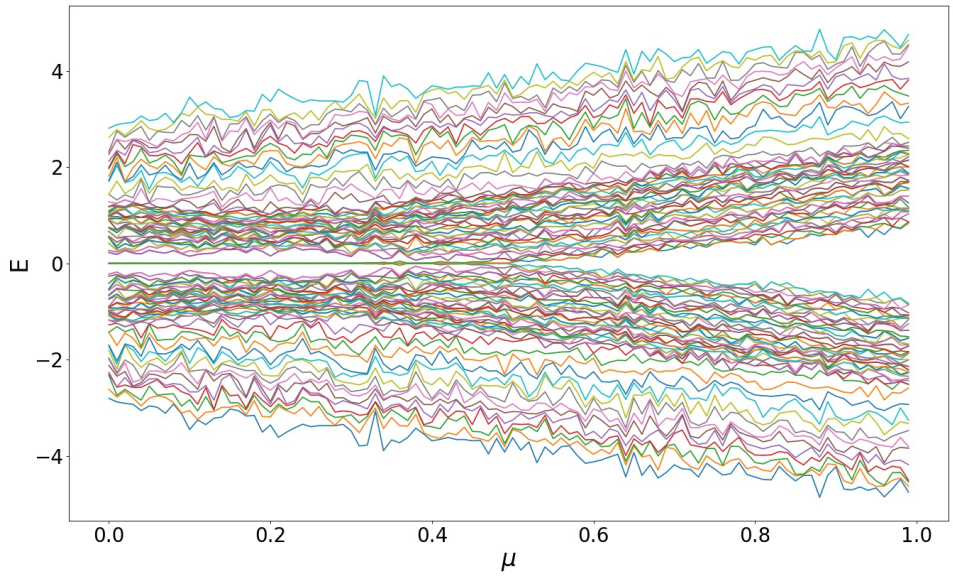

Figure 5.3: Energy E versus hopping μ in the disordered case. We set $t = 0.5$.

5.2.1 Implementing the model and preliminary results

There are some libraries in Python that can make the process of dividing the data into training/test and validation. We used a sequential model from Keras libraries, and a sigmoid function to activate the layers. We used the accuracy to measure the learning ratio, obtaining a value of 95.65%.

A plot with the accuracy vs. epochs is shown in fig. 5.4. We noticed from this learning rate that our NN can recover topological phases from data in real space.

Chapter 6

Conclusions and Perspectives

In the first part of this work, we presented a model for a $1d$ topological Anderson insulator. We started introducing relevant concepts as Anderson localization, scaling hypothesis and topological numbers. Then, we calculated the topological invariant as a second scaling parameter, using the SDRG approach and arrived at the two-parameter flow diagram, completing a scenario proposed by the work in refs. [13] and [17].

In the second part, we went into a different perspective in order to unsderstand how Machine Learning could be useful for classifying topological phases of matter. We showed that in a clean insulator, the supervised algorithm worked really well, in particular our accuracies on training eigenvectors were really high (95.65%). In order to introduce disorder, we needed to calculate the self-energies correction to then re-obtain the topological invariant. There is still a lot to be done in this disordered scenario.

The next step is to make use of other activation functions and train with other types of Neural Networks. We can go even further and build an unsupervised one, and in such case, the topological numbers would be directly predicted from the eigenvectors training.

Bibliography

[1] MÜLLER, C. A.; DELANDE, D. Disorder and interference: localization phenomena. ArXiv preprint: arXiv:1005.0915 (2010).

[2] ANDERSON, P.W. Absence of diffusion in certain random lattices. Physical Review, 109, no. 5, p. 1492 (1958).

[3] THOULESS, D.J., Electrons in Disordered Systems and the Theory of Localization. Physics Reports 13, no. 3, 93-142 (1974).

[4] WEGNER, Franz J., Electrons in disordered systems. Scaling near the mobility edge. Zeitschrift für Physik B Condensed Matter, 25, no. 4, 327-337 (1976).

[5] ABRAHAMS, E., ANDERSON, P. W., LICCIARDELLO, D. C., RAMAKRISHNAN, T. V. (1979). *Scaling theory of localization: Absence of quantum diffusion in two dimensions*. Physical Review Letters, 42(10), 673 (1979).

[6] ASBÓTH, J.K., OROSZLÁNY, L., PÁLYI, A. A short course on topological insulators. Lecture notes in physics, 919 (2016).

[7] KANE, C.L., MELE, E.J. Phys. Rev. Lett., 95, 146802 (2005).

[8] KANE, L., MELE, E.J. Z_2 Topological Order and the Quantum Spin Hall Effect.

[9] RYU, Shinsei, et al. Topological insulators and superconductors: tenfold way and dimensional hierarchy. New Journal of Physics, 12.6: 065010 (2010).

[10] FISHER, Daniel S. Random transverse field Ising spin chains. Physical Review Letters, 69(3):534 (1992).

[11] FISHER, Daniel S. Random antiferromagnetic quantum spin chains. Physical Review B, 50(6):3799 (1994).

[12] FISHER, Daniel S. Critical behavior of random transverse-field Ising spin chains. Physical Review B, 51(10):6411 (1995).

[13] MARD, H. J., HOYOS, J. A., MIRANDA, E., DOBROSAVLJEVIC, V. Strong-disorder renormalization-group study of the one-dimensional tight-binding model. Physical Review B, 90, 125141 (2014).

[14] HUANG, Li, WANG, Lei. Accelerated Monte Carlo simulations with restricted Boltzmann machines. Physical Review B 95.3: 035105 (2017).

[15] CARRASQUILLA, J., MELKO, R. G. Melko. Nature Physics, 13, 431 (2017).

[16] LU, S., HUANG, S., LI, K., LI, J., CHEN, J., LU, D., JI, Z., SHEN, Y., ZHOU, D., ZENG, B. arXiv:1705.0152.

[17] ALTLAND, Alexander; BAGRETS, Dmitry; KAMENEV, Alex. Topology versus Anderson localization: Nonperturbative solutions in one dimension. Physical Review B, 91.8: 085429 (2015).

[18] ALTLAND, A., SIMONS, B. Condensed Matter Field Theory. Cambridge University Press, 2010.

[19] LANDAU, L. D.; LIFSCHITZ E. M., Statistical physics vol.1, 3rd edition. Butterworth-Heinemann (1980).

[20] EVERS, Ferdinand; MIRLIN, Alexander D. Anderson transitions. Reviews of Modern Physics 80, no. 4, 1355 (2008).

[21] SU, W. P., SCHRIEFFER, J. R., HEEGER, A. J. Solitons in polyacetylene, Phys. Rev. Lett., vol. 42, pp. 1698–1701, Jun 1979.

[22] HEEGER, A. J., KIVELSON, S., SCHRIEFFER, J. R., SU, W. P. Su. Solitons in conducting polymers. Rev. Mod. Phys., 60:781, Jul 1988.

[23] MA, S. K.,DASGUPTA, C., HU, C. K., Phys. Rev. Lett., vol. 43, p. 1434 (1979).

[24] PRUISKEN, A. M. M. Phys. Rev. Lett.61,1297 (1988).

[25] BERNEVIG, B. A.; HUGHES, T.L., Topological Insulators and Topological Superconductors. Princeton Press, 2013.

[26] SBIERSKI, Björn; BROUWER, BROUWER, Piet W. $\mathbb{Z}_2$ phase diagram of three-dimensional disordered topological insulators via a scattering matrix approach. Physical Review B, 89.15: 155311 (2014).

[27] VOLOVIK, G. E., The Universe in a Helium Droplet. Oxford University Press, Oxford (2003).

[28] MILLS, K., TAMBLYN, I. arXiv:1706.09779.

[29] MÜLLER, Andreas C., GUIDO, Sarah. Introduction to Machine Learning with Python: A Guide for Data Scientists. O'Reilly Media (2016).

[30] BRUNS, Daniel; HAENEL, Rafael; TOM, Gary. Project 17: Anderson Localization, lecture notes, University of British Columbia, 25 Nov 2017.

[31] ALTLAND, A., BAGRETS, D., FRITZ, L., KAMENEV, A., SCHMIEDT, Hanno. Quantum criticality of quasi-one-dimensional topological Anderson insulators. Physical Review Letters 112, no. 20: 206602 (2014).

[32] LAMACRAFT, A., SIMONS, B. D., ZIRNBAUER, M. R. "Localization from σ-model geodesics." Physical Review B 70.7: 075412 (2004).

[33] LANDAU, L. D. On The Theory of Phase Transitions I, Phys. Z. Sowj. Un.11, 26–47 (1937).

[34] HOLANDA, N. L., GRIFFITH, M. A. Machine learning topological phases in real space. arXiv preprint arXiv:1901.01963 (2019).

[35] ZHANG, P., SHEN, H. and Zhai, H. Machine learning topological invariants with neural networks. Physical review letters, 120(6), p.066401 (2018).

[36] RODRIGUEZ-NIEVA, J.F., SCHEURER, MS. Identifying topological order through unsupervised machine learning. Nature Physics, May 6:1 (2019).

[37] WATT, J., KATSAGGELOS, Borhani R. Machine Learning Refined: Foundations, Algorithms, and Applications. Cambridge University Press (2016).